2007

Skin and Proximity Effects in Two Parallel Plates

Hamdi Eltayib Abdelbagi
Wright State University

SKIN AND PROXIMITY EFFECTS IN TWO PARALLEL PLATES

A thesis submitted in partial fulfillment

of the requirements for the degree of

Master of Science in Engineering

By

Hamdi Altayib Abdelbagi

B.S.EE, 2004

Wright State University

2007

Wright State University

WRIGHT STATE UNIVERSITY

SCHOOL OF GRADUATE STUDIES

August 14, 2007

I HEREBY RECOMMEND THAT THE THESIS PREPARED UNDER MY SUPERVISION BY Hamdi Eltayib Abdelbagi ENTITLED Skin and Proximity Effects in Two Parallel Plates BE ACCEPTED IN PARTIAL FULFILLMENT OF THE REQUIREMENTS FOR THE DEGREE OF Master of Science in Engineering

Marian K. Kazimierczuk, Ph.D.
Thesis Director

Fred D. Garber, Ph.D.
Department Chair

Committee on
Final Examination

Marian K. Kazimierczuk, Ph.D.

Gregory Kozlowski, Ph.D.

Ronald Riechers, Ph.D.

Dr. Josph F. Thomas, Jr, Ph.D.
Dean, School of Graduate Studies

Abstract

Abdelbagi, Hamdi. M.S., Department of Electrical Engineering, Wright State University, 2007. SKIN AND PROXIMITY EFFECTS IN TWO PARALLEL PLATES

Time varying currents within winding and core conductors induce magnetic fields. When more than one conductor is present the resultant magnetic field can be found by adding the individual magnetic fields by superposition. The resultant magnetic field in turn induces eddy currents within each electrical component within the vicinity of the resultant magnetic field. Eddy currents flow in the opposite direction of the primary current and increase the resistance by reducing the area in which the primary current has to travel. Eddy currents also reduce the effectiveness of the conductors to conductor high frequency currents. Skin and proximity effects were numerically investigated for two parallel plate conductors while a laminated core was designed to reduce the power losses. Maxwell's equations were solved to obtain analytical equations for magnetic fields eddy current distribution and power losses. These equations were illustrated in MATLAB for various frequencies to validate the theoretical analysis. Results demonstrate current within an isolated conductor flows near the surface. However, when the same conductor is placed near another conductor the flow path is affected. For the case when the current is flowing in the opposite direction, the magnetic fields are added in the area between the conductors and subtracted on the outer side of the conductor. This causes an increase of the current density within the conductor areas, where the conductors are close to each other. This is the proximity effect. The anti-proximity effect occurs when two conductors carry current in the same direction. In this case the magnetic fields are subtracted from each other in the area between the conductors and are added to each other in the area outside the conductors resulting in a higher current density in these areas. The eddy currents

can be reduced in two ways. Using a highly resistant material for the core increases the skin depth making the distribution of the magnetic flux more uniform. Laminating the core with an oxide film can be used to reduce the eddy current loss as well. The study shows that the eddy current power loss in a sold core is greater than loss in a laminated core by a factor of K^2, where K is the number of the sheets in the laminated core.

Contents

List of Figures

Acknowledgements

I would like to thank my advisor, Dr. Marian K. Kazimierczuk, for his guidance and input on the thesis development process.

I also wish to thank Dr. Gregory Kozlowski and Dr. Ronald Riechers for serving as members of my MS thesis defense committee, giving the constructive criticism necessary to produce a quality technical research document.

I would also like to thank the Department of Electrical Engineering and Dr. Fred D. Garber, the Department Chair, for giving me the opportunity to obtain my MS degree at Wright State University.

I would also like to thank my family, my friends, and Alhamduleelah Wa Alsalat Wa Alsalam Ala Rsoul Allah.

1 Introduction

1.1 Research Background and Motivation of Study

In many electrical devises such as inductors and transformers,there are power losses because electricity converts to heat in their wires. This is one of the main reasons why many devices get hot when they are in use. Studying how the change from electricity to heat occurs and how to reduce the amount of heat released is necessary in order to conserve energy and enhance the operation of electric devices. In power engineering, a conductor is a piece of metal used to conduct electricity, known colloquially as an electrical wire. Conductors have different shapes and sizes. In the United States, smaller conductors are measured by American wire gauges, and large conductors are measured by circular mils. The metal commonly used for conductors is copper because it has high conductivity. Silver is more conductive than copper, but due to cost, it is not practical in most cases and copper is still the most common choice for light-gauge wire. Compared to copper, aluminium has lower conductivity per unit volume, but better conductivity per unit wight. For this reason aluminium is commonly used for large-scale power distribution conductors such as overhead power lines.

However, although many metals have good conductivity, they loose power by converting energy into heat at high frequencies. A conductor and core conductor that carry time-varying currents produce a magnetic field because of its own current, and also it produces another magnetic field because of the currents in adjacent conductors. According to linz's law these magnetic fields produce eddy-current that is opposite to the original current. There are two kinds of eddy-current effects: skin effect and proximity effect. Both of these effects cause nonuniform current density in conductors at high frequencies. The eddy currents flow in the center of the conductor and in the opposite direction to the original current. As a result, the original current tends to

flow near the surface and its density decreases from the surface to the center and increases the (dc) resistance at high frequencies by restricting the conducting area of the wire to the thin skin surface. This is called the skin effect. The proximity effect is similar to the skin effect, but it is caused by the current carried by nearby conductors.

This thesis will focus on the influence of the skin and proximity effects on rectangular conductors and using the lamination method to reduce these effects. The fundamental laws and units of the magnetic theory will be reviewed, magnetic relationships will be given, the equations of the conductors will be derived, and eddy-current losses will be studied. Solutions to reduce the power losses using certain materials on the cores and the lamination method will be provided. Each topic will be discussed using equations, figures, and MATLAB graphs to give a better understanding of the thesis's objectives.

1.2 The Objective

The objectives of this thesis are as follows.

(1) To review and study the skin and proximity effects on the conductors at high frequencies.

(2) To analyze and study the influence of the skin and proximity effects on rectangular conductors, and to interpret high-frequency behaviors.

(4) To analyze the lamination core to in order reduce the eddy-current power loss.

(5) To gain a deep understanding of high-frequency behaviors to obtain a better design in the future to reduce the eddy-current power loss.

1.3 Thesis Outline

The skin and proximity effects are introduced in Chapter 2, and will be explained when and how they occur and how they effect the power loss. Also the skin depth is briefly discussed. In Chapter 3, a deep study of the skin effect on a single rectangular plate is presented, and will use MATLAB simulation to get accurate values and make a better understanding of high-frequency behaviors. The same techniques in Chapter 3 are used in Chapters 4, and 5 to analyze and study proximity and anti-proximity and skin effects in two parallel rectangular plates. In Chapter 6, two solutions are studied to reduce the eddy-current power loss. A high resistivity core and a laminated core are used for this solution. A summary and future work follow in Chapter 7.

2 Skin and Proximity Effects

In order to provide a better understanding of this thesis, skin and proximity effects will be discussed briefly. A winding conductor and core conductor that carry time varying current experience the magnetic field due to its own current and also the magnetic field due to all current carrying conductors in vicinity. In turns, these magnetic fields induce eddy currents in conductors. They oppose the penetration of the conductor by the magnetic field and convert energy into heat. There are two kinds of eddy current effect: skin effect and proximity effect. Both these effects cause non-uniform current density in conductors at high frequencies. These are high frequency phenomena and limit the ability of conductor to conduct high frequency currents. The skin effect and proximity effect are orthogonal to each other and can be considered separately.

2.1 Skin Effect

A time varying currents generate magnetic field that in turn generate currents. The skin effect arises because of the conductor carrying time varying current is immersed in its own magnetic field which, causes eddy current in conductor itself. In accordance with lenz's law, the eddy currents produce a secondary magnetic field that opposes the primary magnetic field. When a time varying AC current flows in conductor, the magnetic field is induced in the conductor by its own current, which causes extra circulating current in the conductor. As a result, the current tends to flow near the surface and the current density tends to decrease from the surface to the center of the conductor. This is called skin effect. As the frequency increases, the conductor effective resistance increases and so does the power loss. At low frequencies, the current takes the path of lowest resistance. At high frequencies, the current takes the path of the lowest inductance. The winding power loss also called the copper loss, is caused by the current flow through the winding resistance. At dc and low

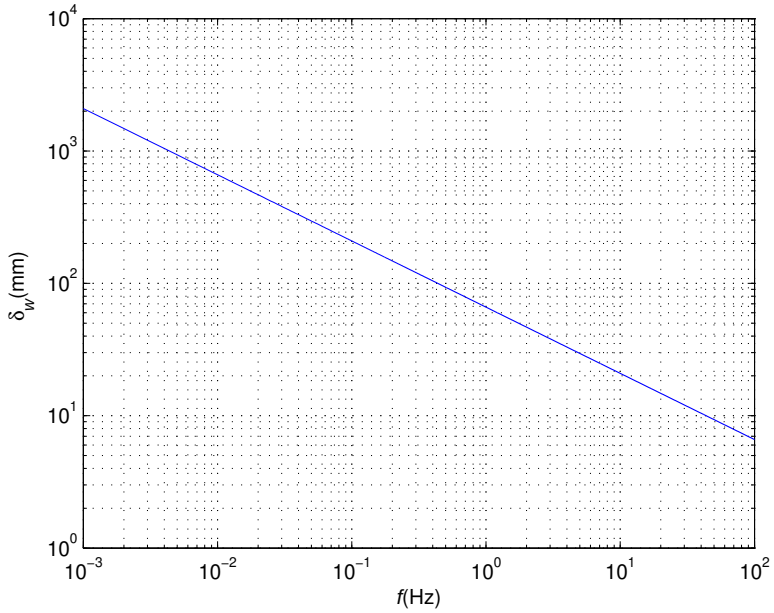

Figure 1: Skin depth δ_w as a function of frequency f .

frequencies, the current density **J** is uniformly distributed throughout the conductor cross-sectional area. when a conducting material is subjected to an alternating magnetic field, eddy current are induced in it. At high frequencies, the current density **J** becomes nonuniform due to eddy currents caused by two mechanisms: the skin effect and proximity effect. Neither the electric field **E** nor the magnetic field **H** penetrate far into a conductor. The point where these fields are reduced by factor $1/e$ is called skin depth δ_w

$$\delta_w = \sqrt{\frac{2}{\omega\mu\sigma}} = \frac{1}{\sqrt{\pi\mu\sigma f}} = \sqrt{\frac{\rho_w}{\pi\mu f}} = \sqrt{\frac{\rho_w}{\pi\mu_r\mu_o f}}. \tag{1}$$

2.2 Proximity Effect

A time varying current i in one conductor generates both external and internal time varying magnetic field H_1. This field in turn induced a time varying current i_2 known as eddy current in nearby conductors, causing power loss. Proximity or closeness of

other current carrying conductor affects the ability of the conductor to carry high frequency current. The magnetic field induced by conductors in close proximity will add or subtract depending in their directions. The proximity effect in inductors and transformers is caused by the time varying magnetic field arising from currents flowing in adjacent winding layers in multiple layer winding. Currents flow in two opposite directions in the same conductor of multiple layer winding, except for the first layer. As a result, the amplitudes and rms values of eddy currents caused by magnetic fields in the adjacent layers due to proximity effect increase significantly as the number of layers N_l increases. Therefore, the power loss due to proximity effect in multiple layer windings is much higher than the power loss in skin effect . In general, the proximity effect occurs when the current in nearby conductors causes a time varying magnetic field and induces a circulating current inside the conductor. The proximity effect is similar to the skin effect, but the difference is that the proximity effect is caused by the current carried by nearby conductors. In the other words, the proximity effect causes magnetic fields due to high frequency currents in one conductor to induce voltages in adjacent winding layers in multi-layer inductor and transformers. Each conductor is subjected to its own field and the fields generated by other conductors. Eddy currents are induced in a conductor by time varying magnetic field whether or not the conductor carries current. If the conductor carries current, the skin effect eddy current and the proximity effect eddy current superimpose to form the total eddy current. If the conductor does not carry current, then only the proximity effect affect eddy current induced. The skin effect current and the proximity effect current are orthogonal. The current density due to the skin effect exhibits an even symmetry and the current density due to the proximity effect exhibits an odd symmetry. The proximity effect causes nonuniform current density in the cross section of the conductors, increasing significantly the winding loss at high frequencies. When

two or more conductors are brought into close proximity, their magnetic fields may add or subtract. The high frequency current will concentrate within a conductor, where the magnetic fields are additive. The magnitude of the proximity effect depend on (1)frequency,(2)conductor geometry (shape and size),(3)arrangement of conductors, and (4)spacing. Mathematically, the proximity effect is very complex.

3 Skin Effect in Single Rectangular Plate

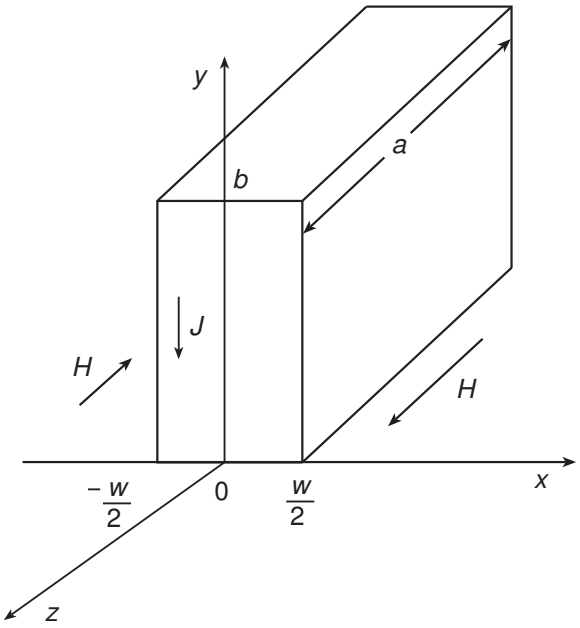

Figure 2: Single isolated plate carrying current

Fig 2 shows a single conducting plate. A sinusoidal current $i(t) = Icoswt$ flows through the plate in $-y$-direction, causing a magnetic field in side and outside the plate in the $y - z$ plate in the z direction for $z > 0$ and in $-z$-direction for $x < 0$. Invoking the odd symmetry of the magnetic field, $H(x) = -H(-x)$ and using Ampere's circuital law

$$\oint_c H \cdot dI = I \tag{2}$$

for the magnetic field intensity on the plate surface, we get

$$aH(\frac{w}{2}) + aH(-\frac{w}{2}) = 1. \tag{3}$$

Assuming that $w << a$ and $w << b$, we obtain the amplitude of the magnetic field intensity at the surface of the plate

$$H(\frac{w}{2}) = -H(-\frac{w}{2}) = \frac{1}{2a} = H_m. \tag{4}$$

The magnetic field intensity H outside the conductor is assumed to be uniform in

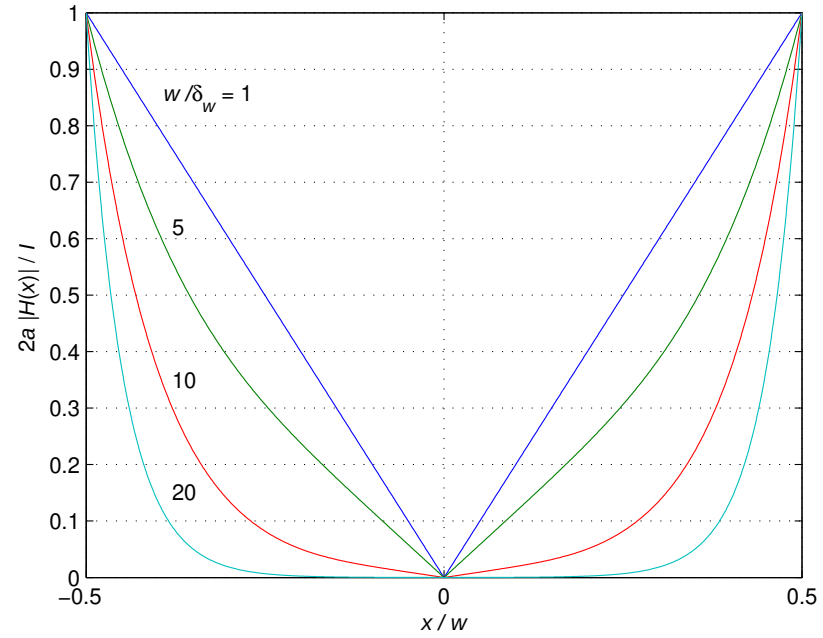

Figure 3: Plot of $2a|H(x)|/I$ as a function of x/w

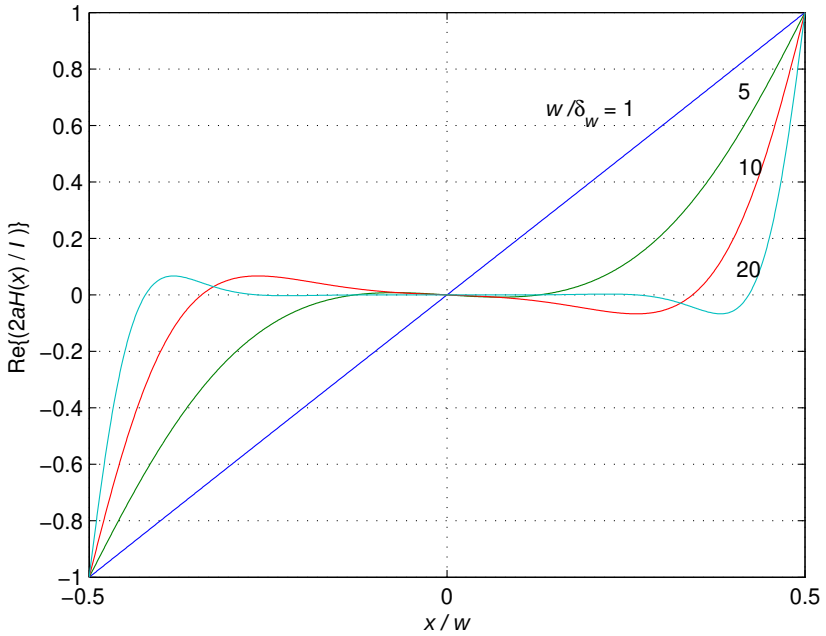

Figure 4: Plot of the real part os $2a|H(x)|/I$ as a function of x/w

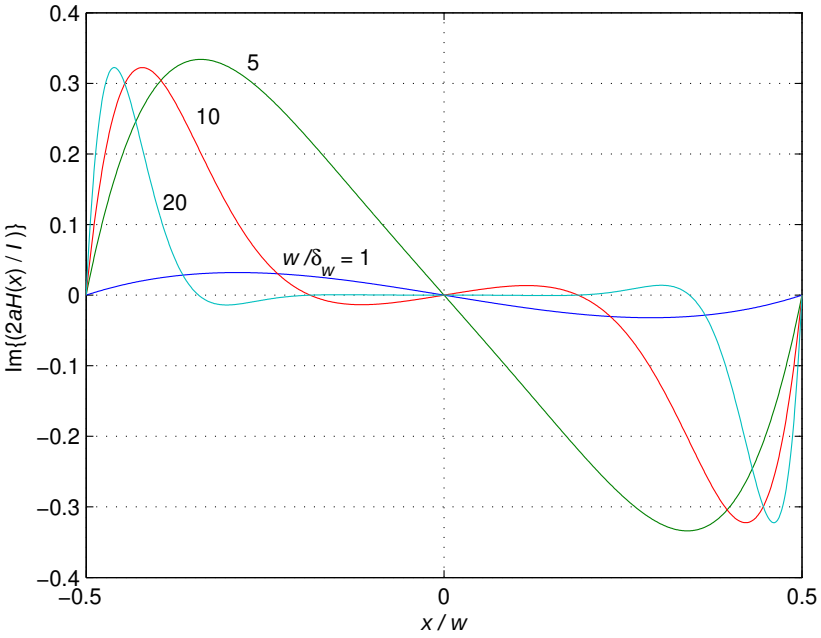

Figure 5: Plot of the imaginary part of $2a|H(x)|/I$ as a function of x/w

the $y-z$ plane and parallel to the current sheet. The magnitude of this field changes only in the x-axis. Therefore, one-dimensional solution is sufficient. The magnetic field is described by the ordinary second-order differential Helmholtz equation,

$$\frac{d^2H(x)}{dx^2} = jw\mu_w\sigma_w H(x) = \gamma^2 H(x) \tag{5}$$

whose general equation is

$$H(x) = H_1 e^{\gamma x} + H_2 e^{-\gamma x}. \tag{6}$$

Form the boundary conditions,

$$H(\frac{w}{2}) = H_1 e^{\gamma \frac{w}{2}} + H_2 e^{-\gamma \frac{w}{2}} \tag{7}$$

and

$$H(-\frac{w}{2}) = H_1 e^{-\gamma \frac{w}{2}} + H_2 e^{\gamma \frac{w}{2}}. \tag{8}$$

Adding these two equations, we obtain

$$H(\frac{w}{2}) + H(-\frac{w}{2}) = (H_1 + H_2)(e^{\gamma x} + e^{-\gamma x}) = 0 \tag{9}$$

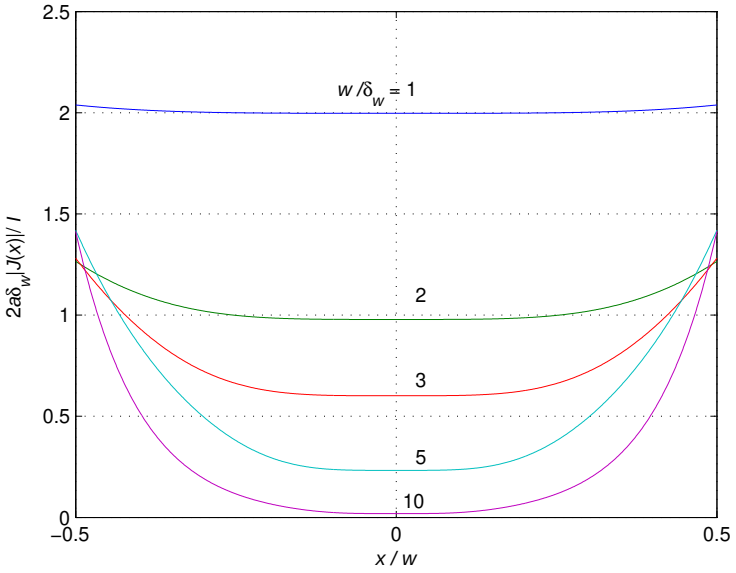

Figure 6: Plot of $2a|J(x)|/I$ as a function of x/w

which produces

$$H_1 = -H_2 = \frac{H_m}{2}. \tag{10}$$

Substitute (10) into (7), we get

$$H(\frac{w}{2}) = H_1(e^{-\gamma\frac{w}{2}} - e^{-\gamma\frac{w}{2}}) = 2H_1\frac{(e^{-\gamma\frac{w}{2}} - e^{-\gamma\frac{w}{2}})}{2} = 2H_1 sinh(\gamma\frac{w}{2}) \tag{11}$$

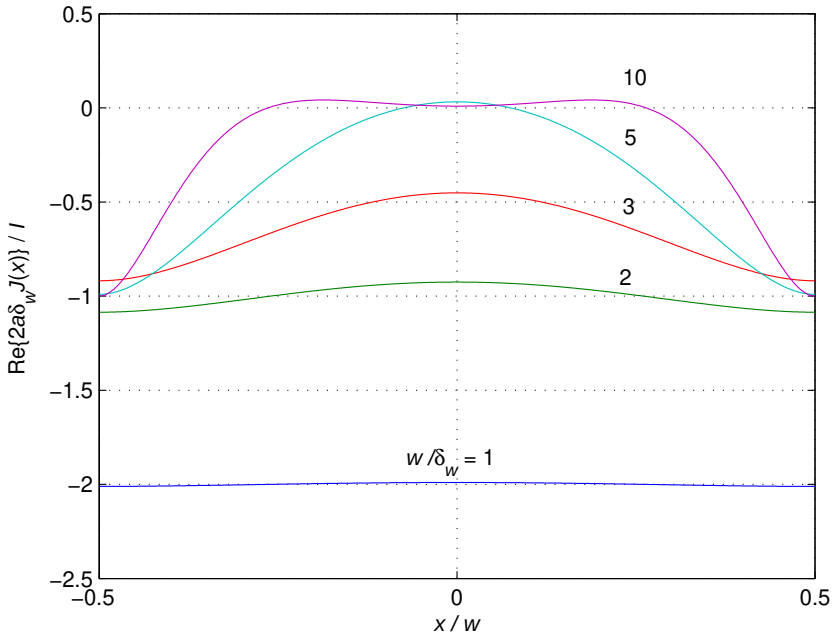

Figure 7: Plot of the real part of $2a|J(x)|/I$ as a function of x/w

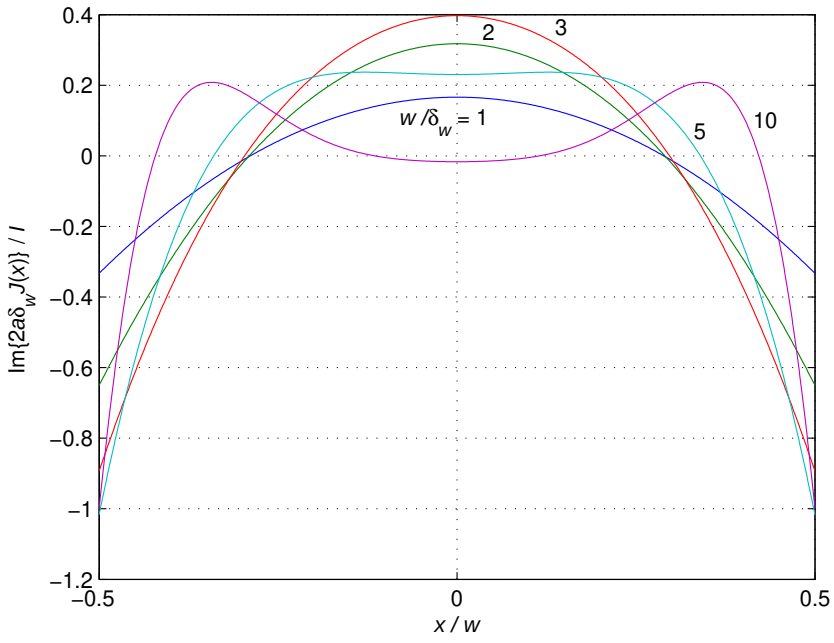

Figure 8: Plot of the imaginary part of $2a|J(x)|/I$ as a function of x/w

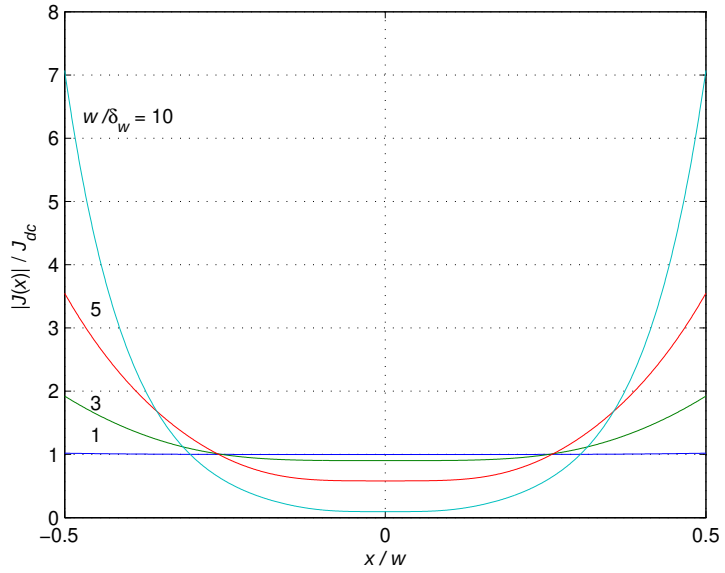

Figure 9: Plot of $J(x)/J_{dc}$ as a function of x/w at selected values for w/δ_w

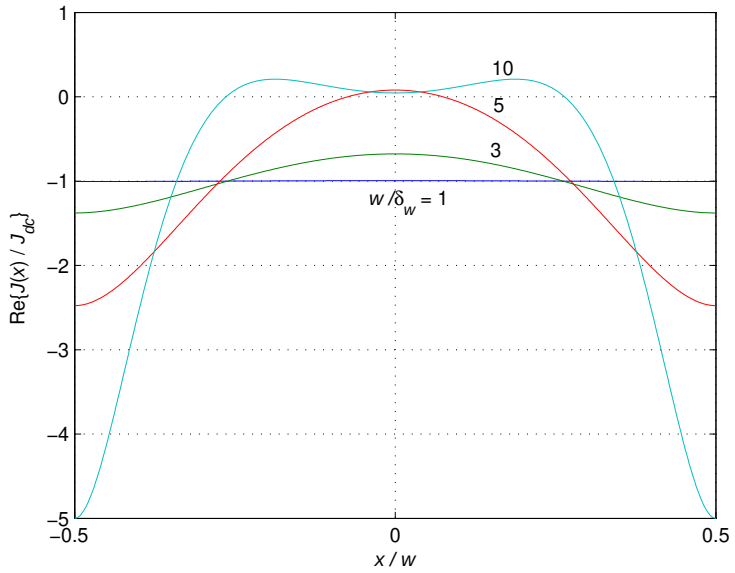

Figure 10: Plot of the real part of $J(x)/J_{dc}$ as a function of x/w at selected values for w/δ_w

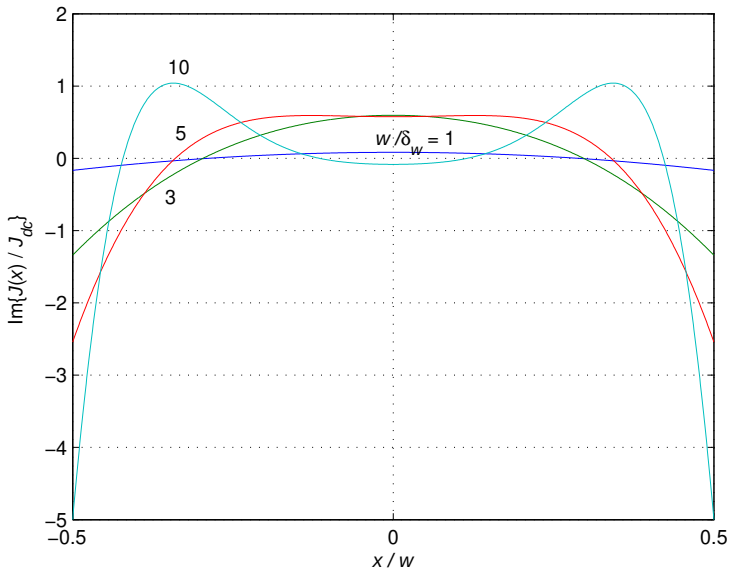

Figure 11: Plot of of the imaginary part of $J(x)/J_{dc}$ as a function of x/w at selected values for w/δ_w

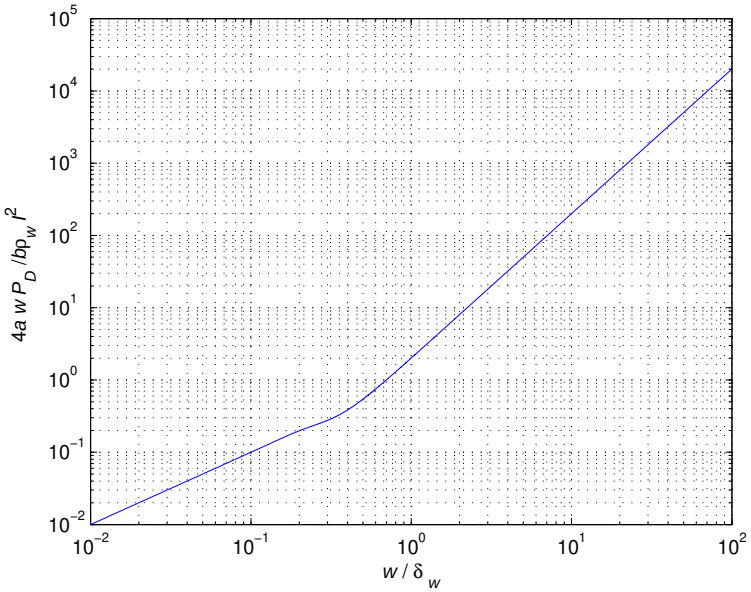

Figure 12: Time-average skin-effect power loss $4awP_D/b\rho_w I^2$ as a function of w/δ_w at fixed δ_w

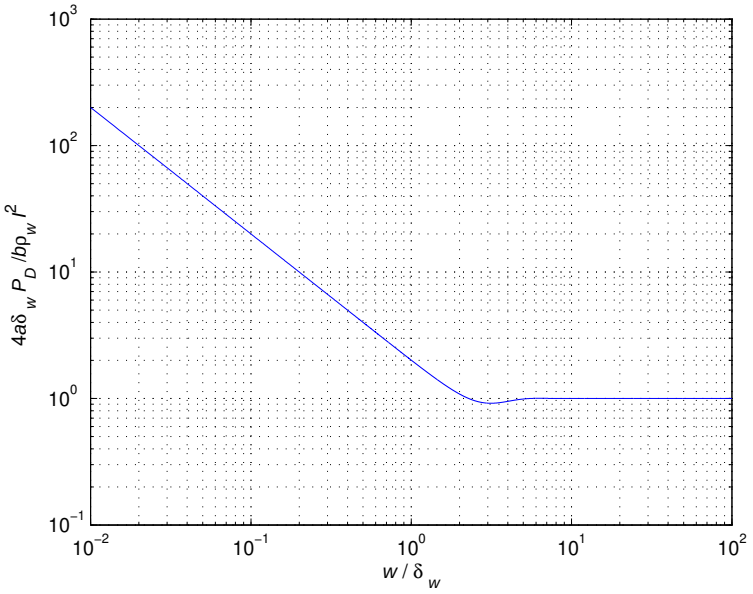

Figure 13: Time-average skin-effect power loss $4a\delta_w P_D/b\rho_w I^2$ as a function of w/δ_w at fixed w

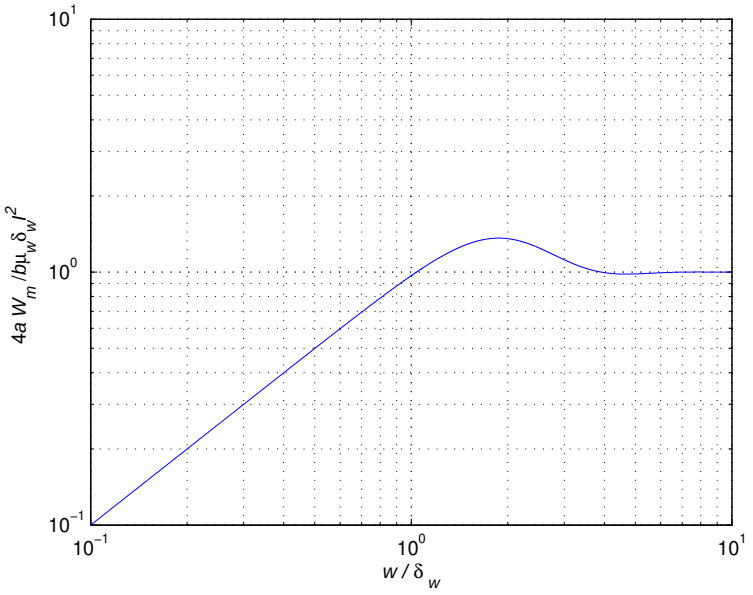

Figure 14: Time-average skin-effect energy stored in the plate $4aW_m/b\delta_w\mu_w I^2$ as a function of w/δ_w

from which

$$H_1 = -H_2 = \frac{H(\frac{w}{2})}{2sinh(\gamma\frac{w}{2})} = \frac{I}{2a}\frac{1}{2sinh(\gamma\frac{w}{2})}. \tag{12}$$

Hence, the magnetic field intensity distribution inside the plate is

$$H(x) = 2H_1\frac{(e^{\gamma\frac{w}{2}} - e^{-\gamma\frac{w}{2}})}{2} = H_m\frac{sinh(\gamma x)}{sinh(\gamma\frac{w}{2})} = \frac{I}{2a}\frac{sinh[(1+j)(\frac{x}{\delta_w})]}{sinh[\frac{(1+j)}{2}(\frac{w}{\delta_w})]}$$

$$= \frac{I}{2a}\frac{sinh[(1+j)(\frac{w}{\delta_w})(\frac{x}{w})]}{sinh[\frac{(1+j)}{2}(\frac{w}{\delta_w})]} \tag{13}$$

Fig. 3, 4, and 5 show plots of $2a\delta_w|H(x)|/I$ and its real and imaginary parts as function of x/w for selected values of w/δ_w.

The current density in the plate is

$$J(x) = J_y(x) = -\frac{dH}{dx} = -\gamma H_m\frac{cosh(\gamma x)}{sinh(\gamma\frac{w}{2})} = -\frac{(1+j)H_m}{\delta_w}\frac{cosh(\gamma x)}{sinh(\gamma\frac{w}{2})}$$

$$= -\frac{(1+j)I}{2a\delta_w}\frac{cosh[(1+j)(\frac{w}{\delta_w})(\frac{x}{w})]}{sinh[\frac{(1+j)}{2}(\frac{w}{\delta_w})]}. \tag{14}$$

Hence,

$$|J(x)| = \frac{I}{2a\delta_w}\frac{cosh(\frac{w}{\delta_w}) + cos(\frac{w}{\delta_w})}{cosh(\frac{w}{\delta_w}) - cos(\frac{w}{\delta_w})}. \tag{15}$$

Fig. 6, 7, and 8 show plots of $2a\delta_w|J(x)|/I$ and its real and imaginary parts as function of x/w for selected values of w/δ_w.

The dc current density in the plate is

$$J_{dc} = \frac{I}{aw}. \tag{16}$$

Hence, the normalized current density is

$$\frac{J(x)}{J_{dc}} = -\frac{(1+j)}{2}(\frac{w}{\delta_w})\frac{cosh[(1+j)(\frac{w}{\delta_w})(\frac{x}{w})]}{sinh[\frac{(1+j)}{2}(\frac{w}{\delta_w})]}. \tag{17}$$

Fig. 9, 10, and 11 show the normalized current density $|J(x)|/J_{dc}$ and its real and imaginary parts as a function of x/w for selected values of w/δ_c. That shows the Ac current almost equal to DC current at low frequencies, and the ratio between the Ac

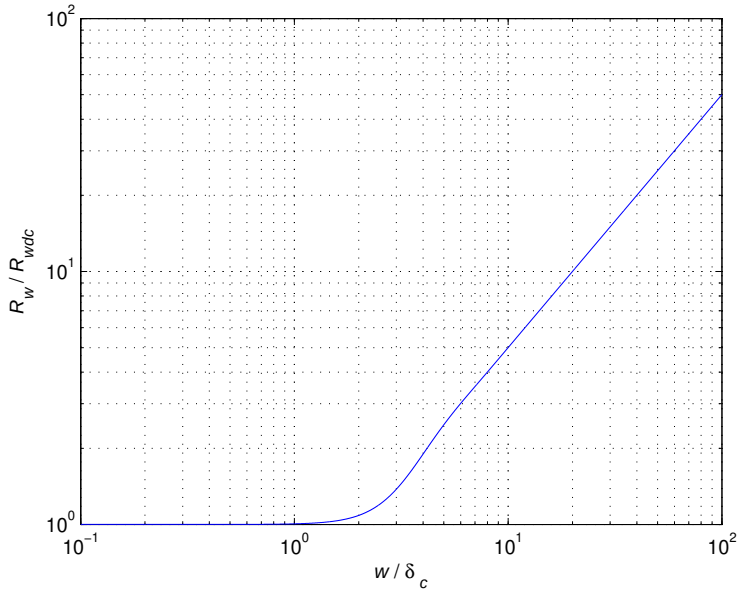

Figure 15: Ratio of R_w/R_{wdc} as a function of w/δ_w

current and DC current increases by increasing the frequency.

The time-average skin-effect power loss at a constant frequency is

$$P_D = \frac{1}{2}\int_0^a \int_0^b \int_{-\frac{w}{2}}^{\frac{w}{2}} \rho_w |J(x)|^2 dxdydz = \frac{\rho_w b I^2}{4a\delta_w} \frac{sinh(\frac{w}{\delta_w}) + sin(\frac{w}{\delta_w})}{cosh(\frac{w}{\delta_w}) - cos(\frac{w}{\delta_w})}. \tag{18}$$

and for varying frequencies is

$$P_D = \frac{\rho_w b I^2}{4a\delta_w} \frac{sinh(\frac{\delta_w}{w}) + sin(\frac{\delta_w}{w})}{cosh(\frac{\delta_w}{w}) - cos(\frac{\delta_w}{w})}. \tag{19}$$

Fig. 12 shows the time-average skin-effect power loss $4a\delta_w P_D/\rho_w b I^2$ as a function of w/δ_w.

Fig 13 shows the time-average skin-effect power loss $4awP_D/\rho_w b I^2$ as a function of w/δ_w.

For high frequencies, $w/\delta_w >> 1$ and values of the hyperbolic are much larger than the values of the trigonometric functions

$$P_D \approx \frac{\rho_w b I^2}{4a\delta_w} = \frac{\rho_w b I^2}{4a}\sqrt{\frac{\pi\mu_w f}{\rho_w}} = \frac{bI^2}{4a}\sqrt{\pi\mu_w f \rho_w}. \tag{20}$$

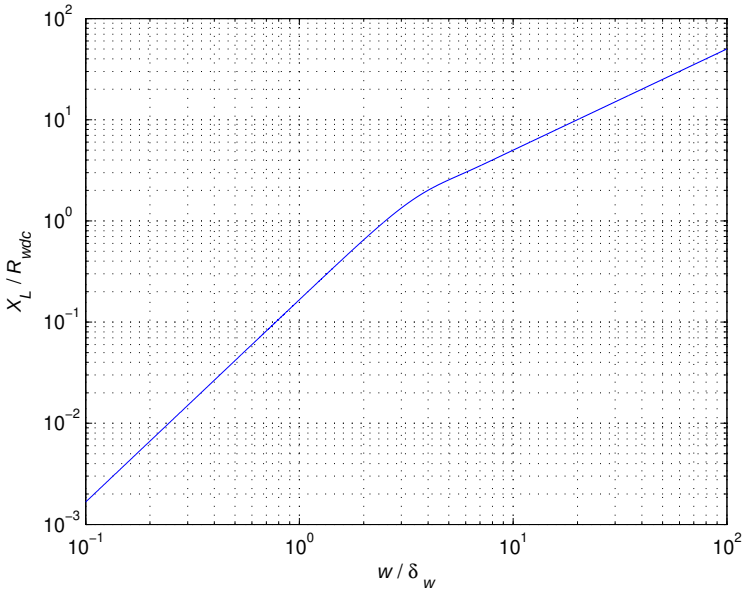

Figure 16: Ratio of X_L/R_{wdc} as a function of w/δ_w

The time-average magnetic energy stored in the plate is

$$W_m = \frac{1}{2}\int\int\int_v \mu_w |H|^2 dV = \frac{\mu_w}{2}\int_0^a\int_0^b\int_{-\frac{w}{2}}^{\frac{w}{2}} \rho_w |H|^2 dxdydz$$

$$= \frac{ab\mu_w}{2}\int_{-\frac{w}{2}}^{\frac{w}{2}} |\frac{I}{2a}\frac{sinh(\gamma x)}{sinh(\gamma\frac{w}{2})}|^2 dx = \frac{\mu_w b\delta_w I^2}{4a}\frac{sinh(\frac{w}{\delta_w}) - sin(\frac{w}{\delta_w})}{cosh(\frac{w}{\delta_w}) - cos(\frac{w}{\delta_w})}. \quad (21)$$

Fig. 14 shows the normalized magnetic energy as a function ofw/δ_w.

The power loss in the plate at any frequency can be expressed as

$$P_D = \frac{1}{2}I^2 R_w = \frac{1}{2}I^2\frac{\rho_w b}{2a\delta_w}\frac{sinh(\frac{w}{\delta_w}) + sin(\frac{w}{\delta_w})}{cosh(\frac{w}{\delta_w}) - cos(\frac{w}{\delta_w})} \quad (22)$$

yielding the resistance at any frequency

$$R_w = \frac{\rho_w b}{2aw\delta_w}\frac{w}{\delta_w}\frac{sinh(\frac{w}{\delta_w}) + sin(\frac{w}{\delta_w})}{cosh(\frac{w}{\delta_w}) - cos(\frac{w}{\delta_w})} \quad (23)$$

The dc resistance of the plate is

$$R_{wdc} = \rho_w\frac{b}{aw}. \quad (24)$$

The ratio of the resistance at any frequency to the dc resistance is

$$F_R = \frac{R_w}{R_{wdc}} = \frac{1}{2}\frac{w}{\delta_w}\frac{sinh(\frac{w}{\delta_w}) + sin(\frac{w}{\delta_w})}{cosh(\frac{w}{\delta_w}) - cos(\frac{w}{\delta_w})} \quad (25)$$

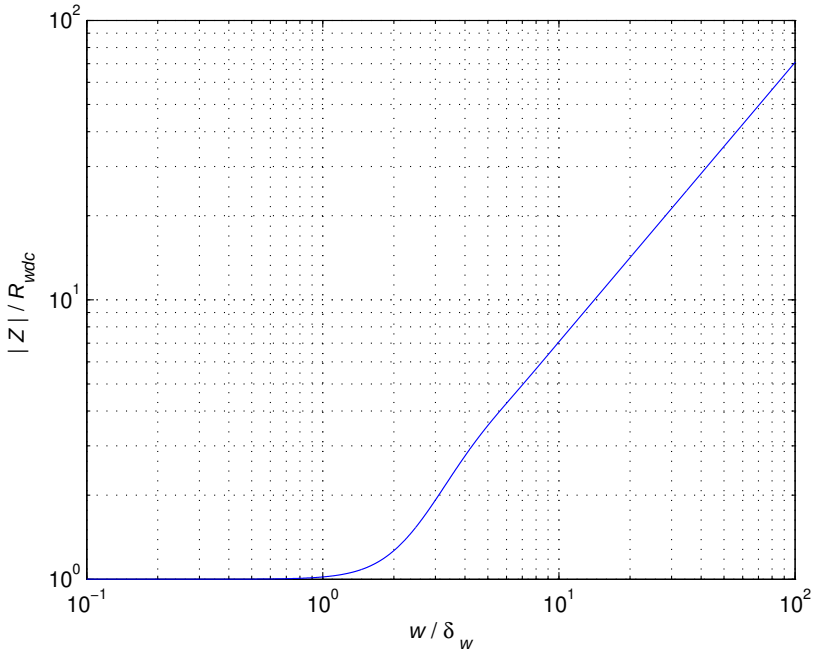

Figure 17: Plot of $|Z|/R_{wdc}$ as a function of w/δ_w

Fig. 15 shows the ratio of R_w/R_{wdc} as a Function of w/δ_w.

Assuming that the current flows uniformly over the skin depth δ_w only near both surfaces of the effective area $A_e = 2\delta_w a$, the plate ac resistance at hight frequencies is

$$R_w \approx \frac{\rho_w b}{2a\delta} \approx \frac{b}{2a}\sqrt{\pi\mu_w\rho_w f} \tag{26}$$

$$F_R = \frac{R_w}{R_{wdc}} = \frac{w}{2\delta_w} = \frac{b}{2}\sqrt{\frac{\pi\mu_0 f}{\rho_w}}. \tag{27}$$

The magnetic energy stored inside the plate can be expressed as

$$\frac{1}{2}LI^2 = \frac{\mu_w b\delta_w I^2}{4a}\frac{sinh(\frac{w}{\delta_w}) - sin(\frac{w}{\delta_w})}{cosh(\frac{w}{\delta_w}) - cos(\frac{w}{\delta_w})} \tag{28}$$

yielding the internal inductance

$$L = \frac{X_L}{w} = \frac{\mu_w b\delta_w}{2a}\frac{sinh(\frac{w}{\delta_w}) - sin(\frac{w}{\delta_w})}{cosh(\frac{w}{\delta_w}) - cos(\frac{w}{\delta_w})} \tag{29}$$

The reactance X_L due to the internal inductance L normalized with respect to the

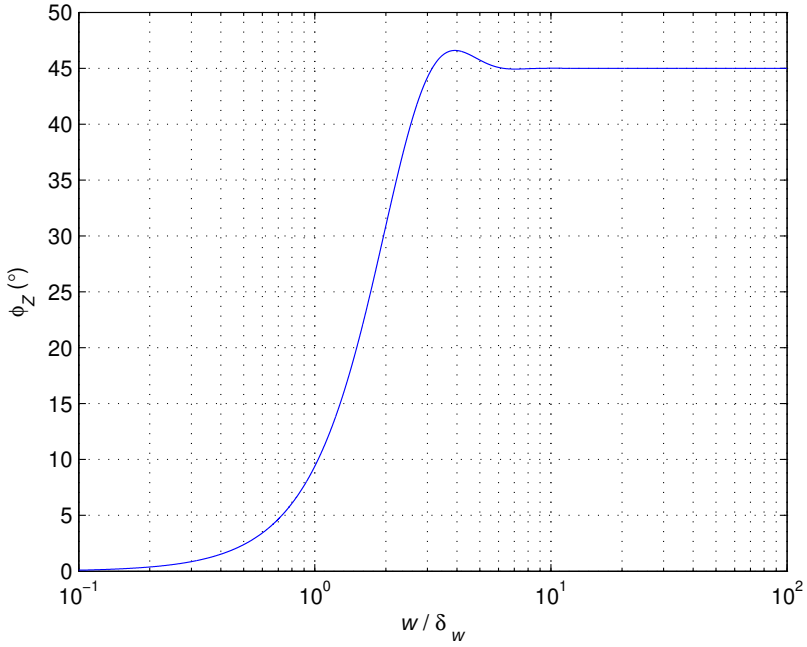

Figure 18: Ratio of ϕ_Z as a function of w/δ_w

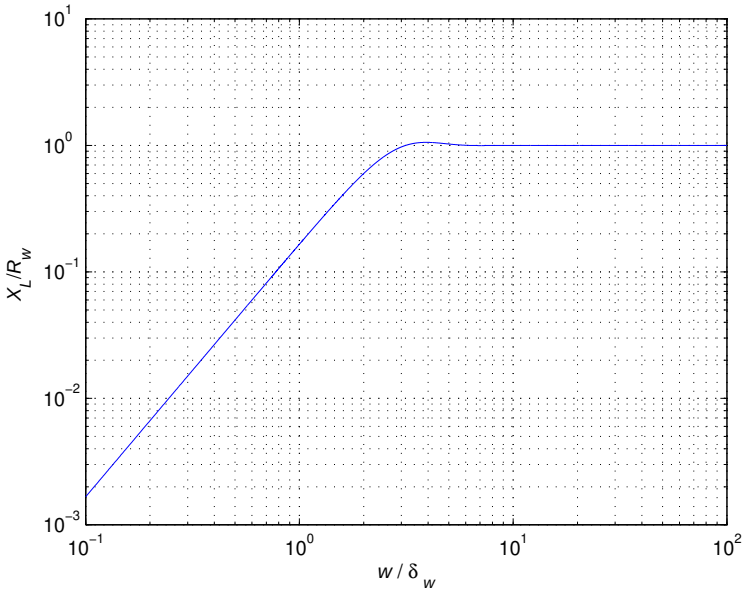

Figure 19: Ratio of X_L/R_w as a function of w/δ_w

dc resistance R_{wdc} is given by

$$F_X = \frac{X_L}{R_{wdc}} = \frac{1}{2}\frac{w}{\delta_w}\frac{sinh(\frac{w}{\delta_w}) - sin(\frac{w}{\delta_w})}{cosh(\frac{w}{\delta_w}) - cos(\frac{w}{\delta_w})}. \tag{30}$$

Fig. 16 shows the ratio X_L/R_{wdc} as a function of w/δ_w. The total internal impedance is

$$Z = \frac{1}{2}R_{wdc}(\frac{w}{\delta_w})\left[\frac{sinh(\frac{w}{\delta_w}) - sin(\frac{w}{\delta_w})}{cosh(\frac{w}{\delta_w}) - cos(\frac{w}{\delta_w})} + j\frac{sinh(\frac{w}{\delta_w}) - sin(\frac{w}{\delta_w})}{cosh(\frac{w}{\delta_w}) - cos(\frac{w}{\delta_w})}\right]$$
$$= R_{wdc} + jX_L = |Z|e^{j\phi z} \tag{31}$$

Figs. 17 and 18 show $|Z|/R_{wdc}$ and ϕ_z as function of w/δ_w.

Fig. 19 shows the ratio of X_L/R_w. An alternative method of deriving an expression for the plate impedance is given below. The electric field intensity is given by

$$E = \rho_w J = \rho_w \frac{dH}{dx} = -\frac{\rho_w \gamma I}{2a}\frac{cosh(\gamma x)}{sin(\gamma\frac{w}{2})}. \tag{32}$$

The plate impedance is

$$Z = \frac{V}{I} = \frac{bE\frac{w}{2}}{I} = \frac{b\rho_w\gamma}{2a}coth(\gamma\frac{w}{2}) = \frac{b\rho_w}{2a\delta_w}(1+j)coth(\gamma\frac{w}{2})$$
$$= \frac{1}{2}R_{wdc}(\frac{w}{\delta_w})(1+j)coth(\gamma\frac{w}{2}) = R + jX_L. \tag{33}$$

Using the relation

$$coth(1+j)x = \frac{sinh2x - jsin2x}{cosh2x - cos2x} \tag{34}$$

we obtain the same result in equation (30)

4 Proximity and Skin Effects in Two Parallel Plates

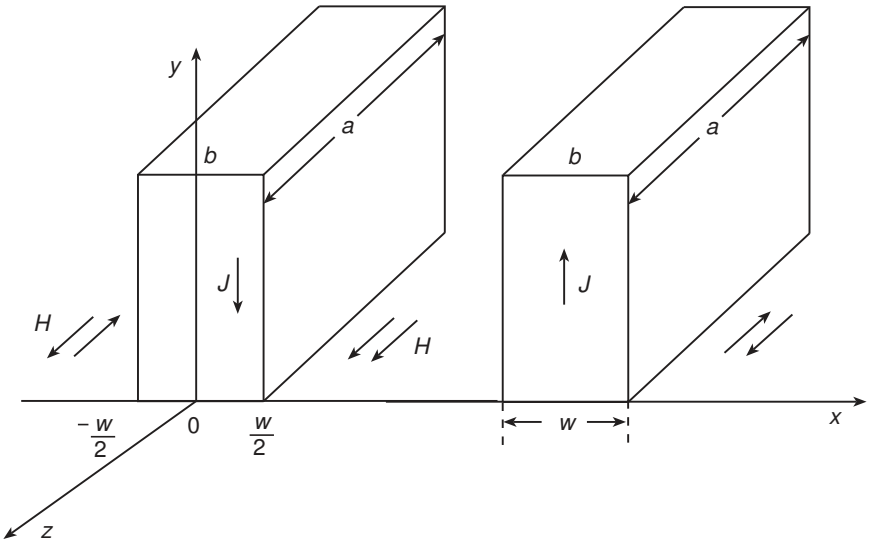

Figure 20: Two plates carrying currents in opposite directions.

Fig. 20 shows two parallel rectangular conducting plates. Considering the case in which the currents $i(t) = Icoswt$ flow in the plates in opposite directions. The current in the left plate flows in the $-y$-directions and in the right plate in the $y-$direction. The currents cause the magnetic field inside and outside the plates. The magnetic fields generated by both plates add up between the plates, causing larger current density $j(x)$ in the plate areas, where the plates are close to each others. Using Ampere's circuital law,

$$\oint_c H \cdot dI = I \tag{35}$$

we have

$$aH(\frac{w}{2}) - aH(-\frac{w}{2}) = aH(\frac{w}{2}) = 1 \tag{36}$$

because

$$H(-\frac{w}{2}) = 0. \tag{37}$$

thus,

$$H_m = H(\frac{w}{2}) = \frac{1}{a}. \tag{38}$$

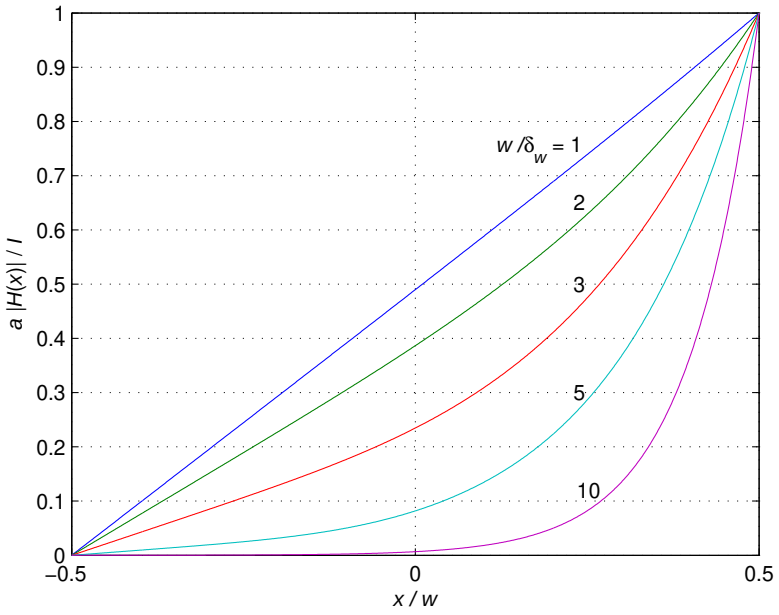

Figure 21: Plot of $a|H(x)|/I$ as a function of x/w for selected values of w/δ_w in the left plate due to the proximity effect.

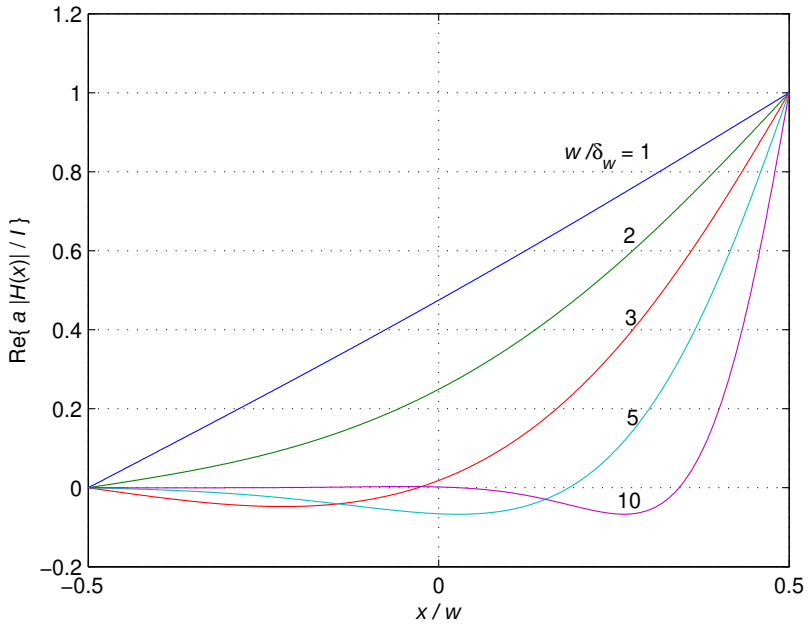

Figure 22: Plot of the real part of $a|H(x)|/I$ as a function of x/w for selected values of w/δ_w. The current density is given by in the left plate due to the proximity effect.

The magnetic field inside the plates is described by the Helmholtz equation

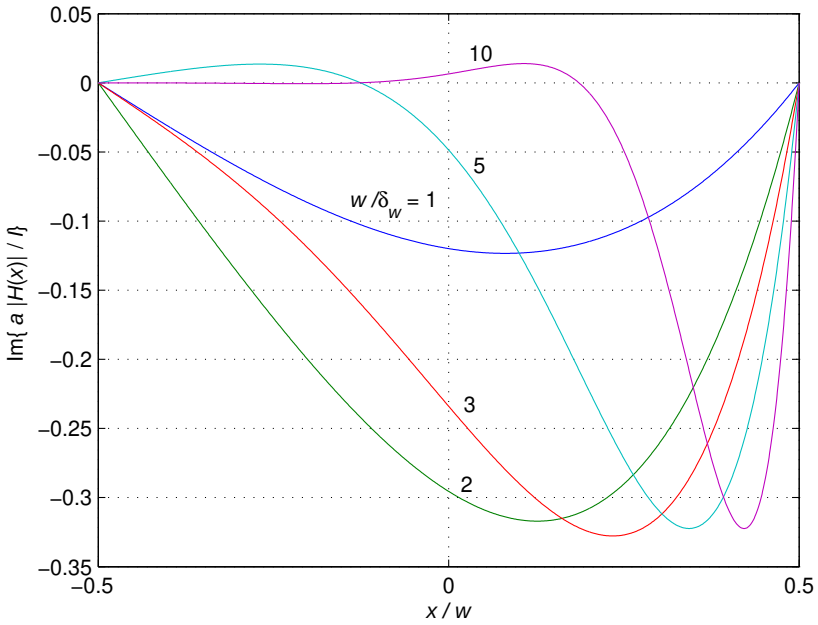

Figure 23: Plot of the imaginary part of $a|H(x)|/I$ as a functed of x/w for selection values of w/δ_w. The current density is given by in the left plate due to the proximity effect.

$$\frac{d^2H(x)}{dx^2} = jw\mu_w\sigma_w H(x) = \gamma^2 H(x). \tag{39}$$

whose general solution is

$$H(x) = H_1 e^{\gamma x} + H_2 e^{-\gamma x}. \tag{40}$$

From the boundary conditions,

$$H(\frac{w}{2}) = H_1 e^{\gamma\frac{w}{2}} + H_2 e^{-\gamma\frac{w}{2}} = \frac{1}{a} \tag{41}$$

and

$$H(-\frac{w}{2}) = H_1 e^{-\gamma\frac{w}{2}} + H_2 e^{\gamma\frac{w}{2}} = 0. \tag{42}$$

hence,

$$H_2 = -H_1 e^{-\gamma w} \tag{43}$$

producing

$$H_1 = \frac{1}{a}\frac{e^{\gamma\frac{w}{2}}}{e^{\gamma w} - e^{-\gamma w}} \tag{44}$$

and

$$H_2 = -\frac{1}{a}\frac{e^{-\gamma\frac{w}{2}}}{e^{\gamma w} - e^{-\gamma w}} \tag{45}$$

The magnetic field is given by

$$H(x) = \frac{I}{a}\frac{sinh[\gamma(x+\frac{w}{2})]}{sinh(\gamma w)}. \tag{46}$$

Fig. 21, 22 and 23 shows plots of $a|H(x)|/I$ and its real and imaginary parts as a function of x/w for selection values of w/δ_w.

The current density is given by

$$J(x) = -\frac{dH(x)}{dx} = -\frac{\gamma I}{a}\frac{cosh[\gamma(x+\frac{w}{2})]}{sinh(\gamma w)}. \tag{47}$$

Fig. 24, 25 and 26 show plots of $a|(Jx)|/I$ and its real and imaginary parts as a function of x/w for selection values of w/δ_w.

The dc current density in each plate is

$$J_{dc} = \frac{I}{aw}. \tag{48}$$

Hence, the normalized current density in the plate is

$$\frac{J(x)}{J_{dc}} = w\gamma - \frac{cosh[\gamma(x+\frac{w}{2})]}{sinh(\gamma w)} = -(1+j)(\frac{w}{\delta_w})\frac{cosh[\gamma(x+\frac{w}{2})]}{sinh(\gamma w)}. \tag{49}$$

Fig. 27, 28 and 29 show normalized current density of $|J(x)|/J_{dc}$ and its real and imaginary parts as a function of x/w for selection values of w/δ_w. The current density due to skin and proximity effects at the surfaces of the conductor for $x = w/2$ and $x = -w/2$ is given by

Fig. 30 shows plot of $P(x)/\rho_w$ for selection values of w/δ_w in the left plate due to the proximity effect.

$$J_{sp}(\frac{w}{2}) = -\frac{\gamma I}{a}\frac{cosh(\gamma w)}{sinh(\gamma w)}. \tag{50}$$

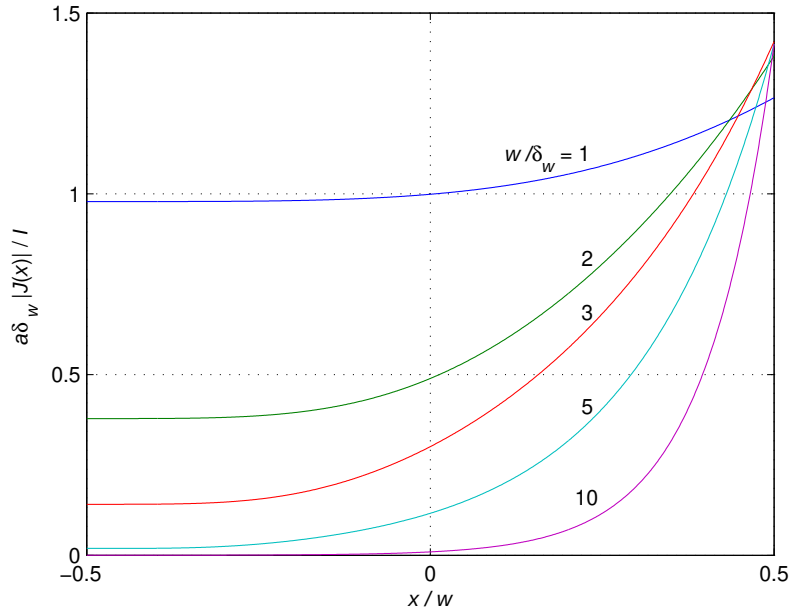

Figure 24: Plot of $a|J(x)|/I$ as a function of x/w for selected values of w/δ_w in the left plate due to the proximity effect.

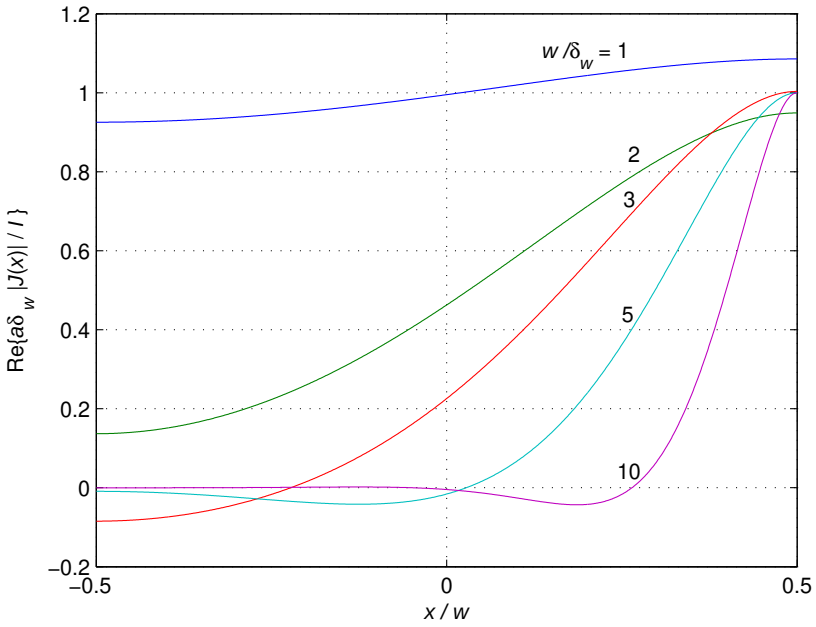

Figure 25: Plot of the real part of $a|J(x)|/I$ as a function of x/w for selected values of w/δ_w in the left plate due to the proximity effect.

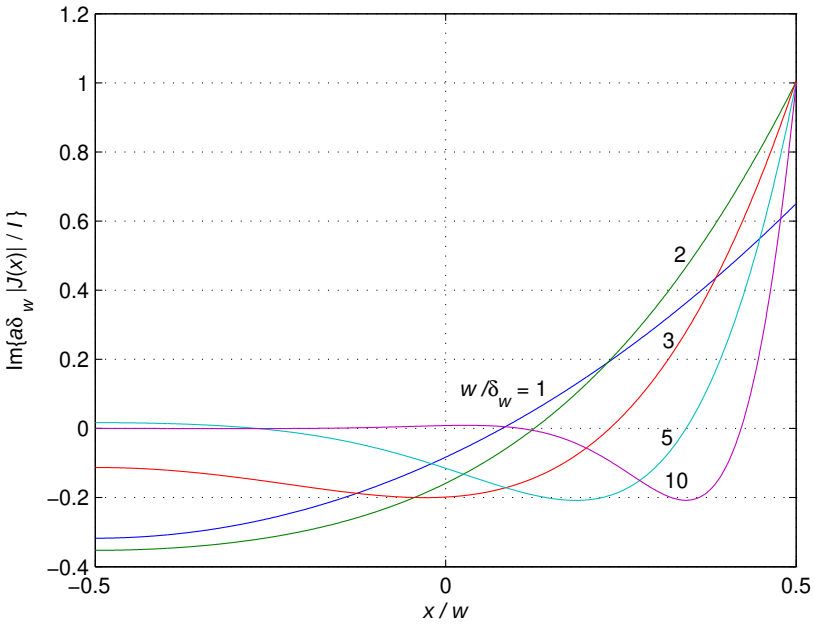

Figure 26: Plot of the imaginary part of $a|J(x)|/I$ as a function of x/w for selected values of w/δ_w in the left plate due to the proximity effect.

and

$$J_{sp}(-\frac{w}{2}) = -\frac{\gamma I}{a}\frac{1}{sinh(\gamma w)}. \tag{51}$$

The current density due to the skin effect only for $x = w/2$ and $x = 0$ is

$$J_s(\frac{w}{2}) = -\frac{\gamma I}{2a}\frac{cosh(\gamma\frac{w}{2})}{sinh(\gamma\frac{w}{2})} \tag{52}$$

and

$$J_s(0) = J_{sp}(0) = -\frac{\gamma I}{2a}\frac{1}{sinh(\gamma\frac{w}{2})}. \tag{53}$$

Hence,

$$\frac{J_{sp}(-\frac{w}{2})}{J_s(-\frac{w}{2})} = \frac{1}{1 + sinh^2(\gamma\frac{w}{2})} \tag{54}$$

$$\frac{J_{sp}(\frac{w}{2})}{J_s(\frac{w}{2})} = 1 + tanh^2(\gamma\frac{w}{2}) \tag{55}$$

and

$$\frac{J_{sp}(0)}{J_s(0)} = 1. \tag{56}$$

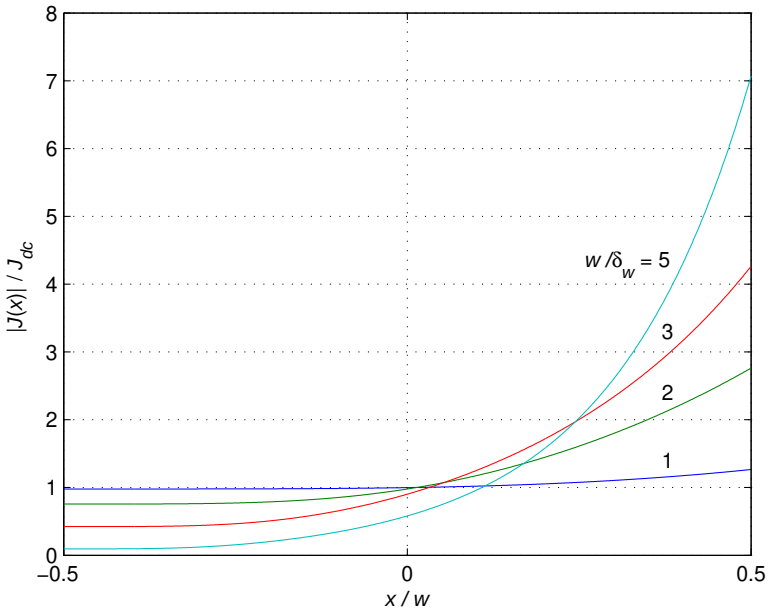

Figure 27: Plot of $|J(x)|/J_{dc}$ as a function of x/w for selected values of w/δ_w in the left plate due to the proximity effect.

Fig. 31 and 32 show plots of$|J_{sp}(-w/2)|/J_s(-w/2)$ and $|J_{sp}(w/2)|/J_s(w/2)$ as function of w/δ_w. The power density distribution is given by

$$P(x) = \frac{1}{2}\rho_w|J(x)|^2 = \frac{1}{2}\frac{\rho_w I^2}{a^2}\left|\frac{\gamma cosh[\gamma(x+\frac{w}{2})]}{sinh(\gamma w)}\right|^2. \tag{57}$$

The total power loss in each conductor due to the proximity and skin effects at a constant frequency is

$$P_{sp} = \frac{1}{2}\int\int\int_v \rho_w|J(x)|^2 dV = \frac{\rho_w}{2}\int_0^a\int_0^a\int_{-fracw2}^{fracw2}\frac{I^2}{a^2}\left|\gamma\frac{cosh[\gamma(x+\frac{w}{2})]}{sinh(\gamma w)}\right| dxdydz$$

$$= \frac{\rho_w b I^2}{2a\delta_w}\frac{sinh(\frac{2w}{\delta_w})+sin(\frac{2w}{\delta_w})}{cosh(\frac{2w}{\delta_w})-cos(\frac{2w}{\delta_w})}. \tag{58}$$

and at varying frequencies is

$$P_{sp} = \frac{\rho_w b I^2}{2a\delta_w}\frac{sinh(\frac{\delta_w}{2w})+sin(\frac{\delta_w}{2w})}{cosh(\frac{\delta_w}{2w})-cos(\frac{\delta_w}{2w})}. \tag{59}$$

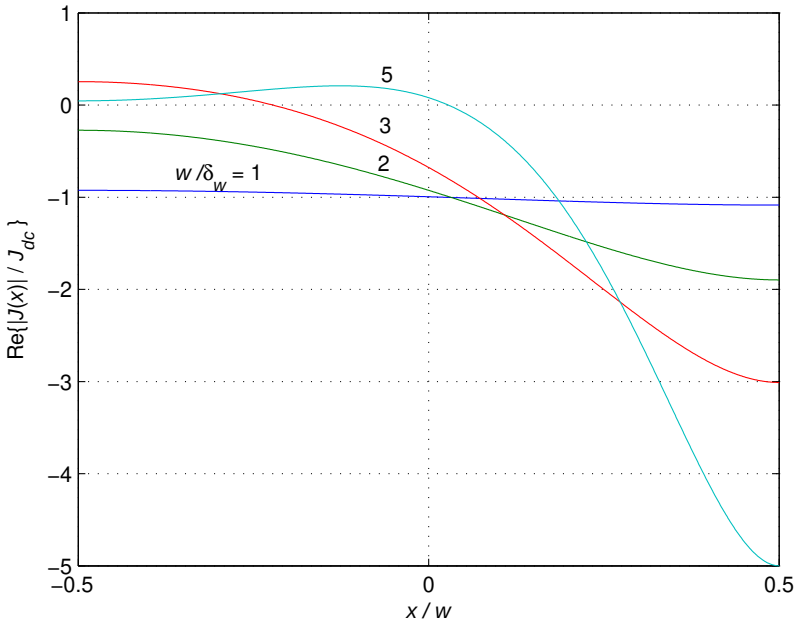

Figure 28: Plot of the real part of $|J(x)|/J_{dc}$ as a function of x/w for selected values of w/δ_w in the left plate due to the proximity effect.

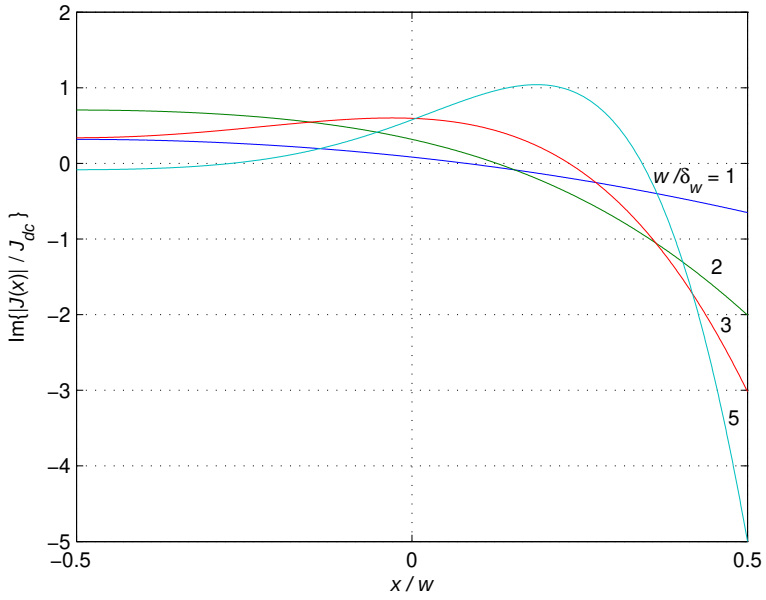

Figure 29: Plot of the imaginary part of $|J(x)|/J_{dc}$ as a function of x/w for selected values of w/δ_w in the left plate due to the proximity effect.

Fig. 33 shows the power loss due to skin and proximity effect $awP_{sp}/b\rho_w I^2$ as a function of w/δ_w.The plot shows that when the frequency increases, the power loss due to skin and proximity effects also increases.

Fig. 34 shows the power loss due to skin and proximity effect $a\delta_w P_{sp}/b\rho_w I^2$ as a function of w/δ_w. The plot shows that when the width of the plate increases, the power loss due to skin and proximity effects decreases.

The power due to the skin effect at a constant frequency is the same at that for a single plate and it is given by

$$P_s = \frac{\rho_w b I^2}{4a\delta_w} \frac{sinh(\frac{2w}{\delta_w}) + sin(\frac{2w}{\delta_w})}{cosh(\frac{2w}{\delta_w}) - cos(\frac{2w}{\delta_w})}. \tag{60}$$

and for varying frequencies is

$$P_s = \frac{\rho_w b I^2}{4a\delta_w} \frac{sinh(\frac{\delta_w}{2w}) + sin(\frac{\delta_w}{2w})}{cosh(\frac{\delta_w}{2w}) - cos(\frac{\delta_w}{2w})}. \tag{61}$$

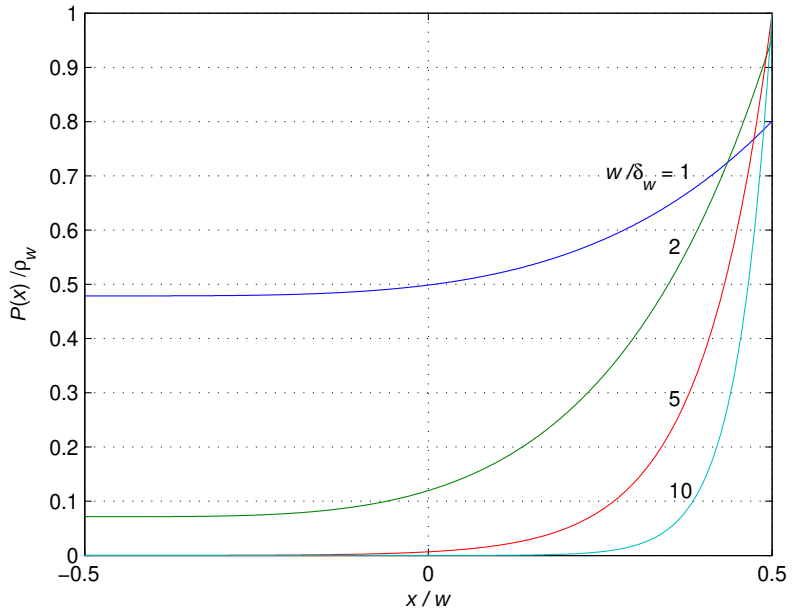

Figure 30: Plots of $P(x)/\rho_w$ as a function of x/w for selected values of w/δ_w in the left plate due to the proximity effect.

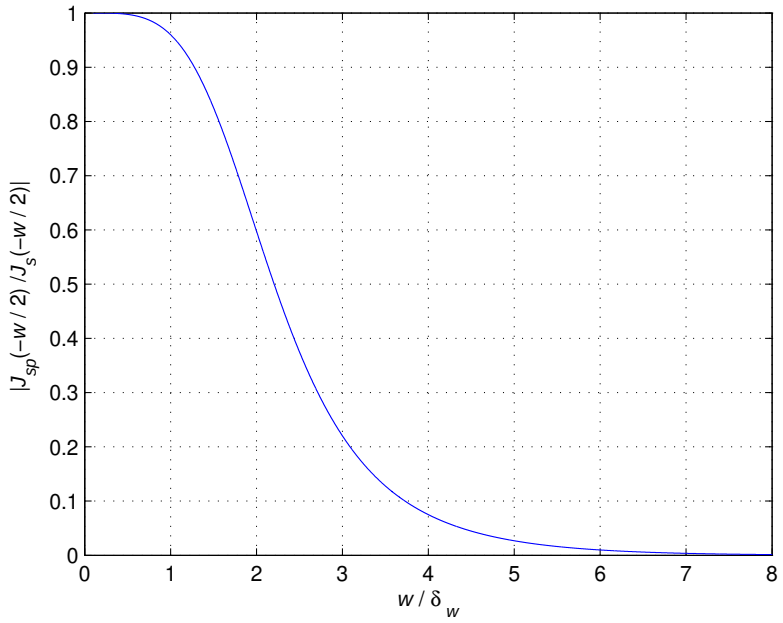

Figure 31: Plots of $|J_{sp}(-w/2)/J_s(-w/2)|$ as a function of w/δ_w .

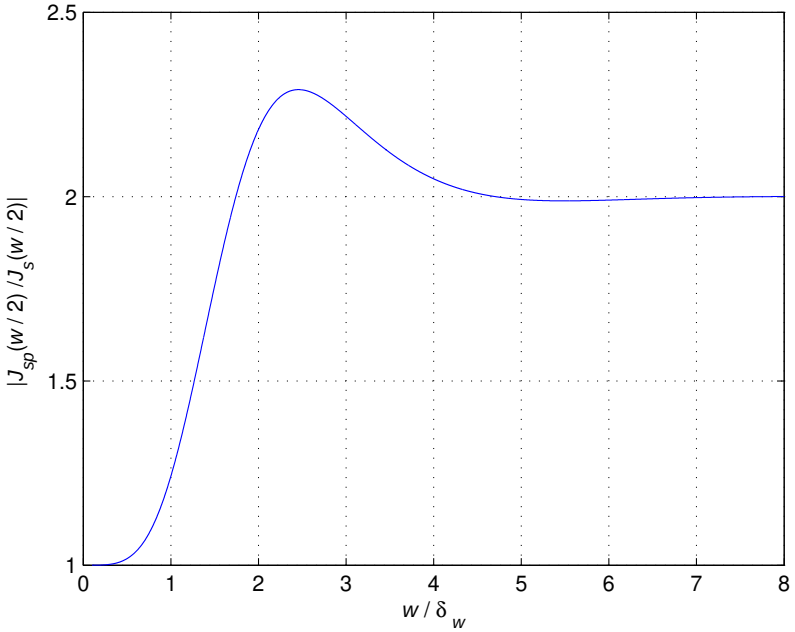

Figure 32: Plot of $|J_{sp}(w/2)/J_s(w/2)|$ as a function of w/δ_w .

The proximity loss is:

$$P_p = P_{ps} - P_s = \frac{\rho_w b I^2}{4a\delta_w} \frac{sinh(\frac{\delta_w}{2w}) - sin(\frac{\delta_w}{2w})}{cosh(\frac{\delta_w}{2w}) + cos(\frac{\delta_w}{2w})}. \tag{62}$$

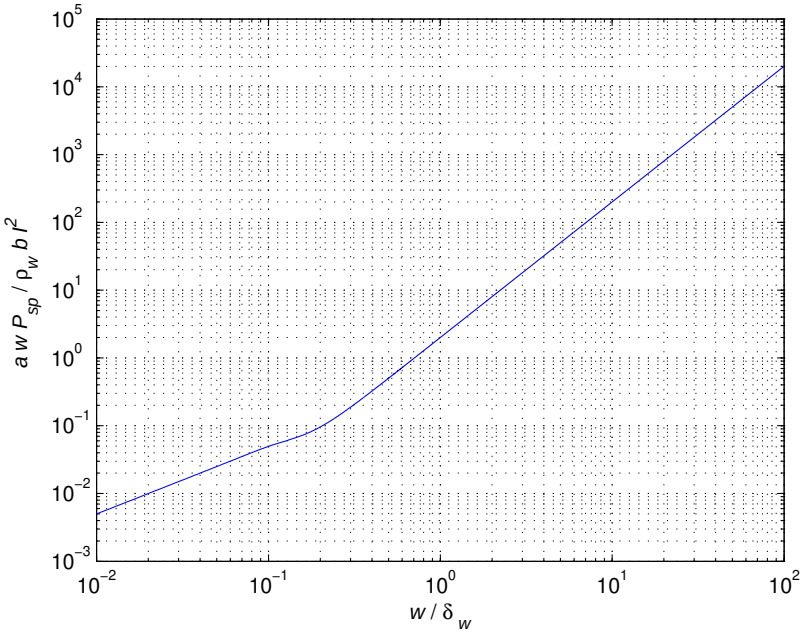

Figure 33: Plot of the power loss due to skin and proximity effects $awP_{sp}/b\rho_w I^2$ as a function of w/δ_w at fixed w.

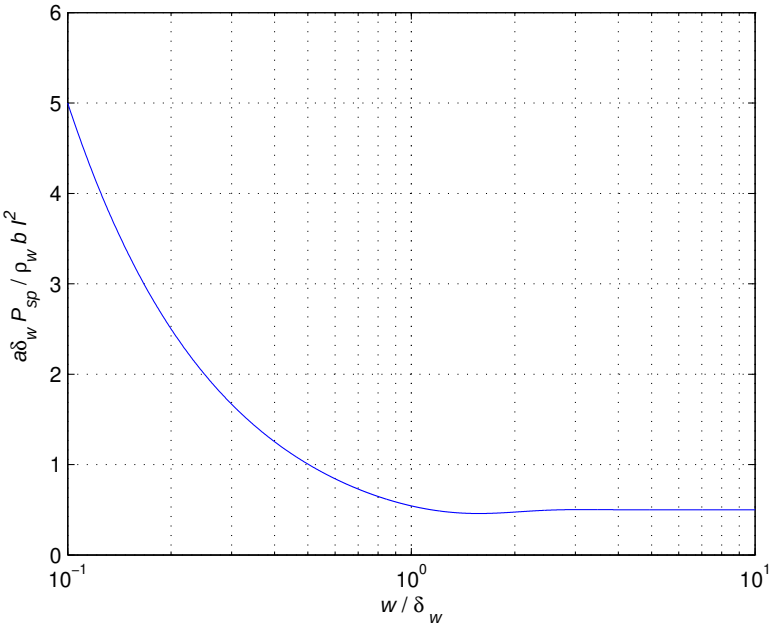

Figure 34: Plot of the power loss due to skin and proximity effects $a\delta_w P_{sp}/b\rho_w I^2$ as a function of w/δ_w at fixed δ_w .

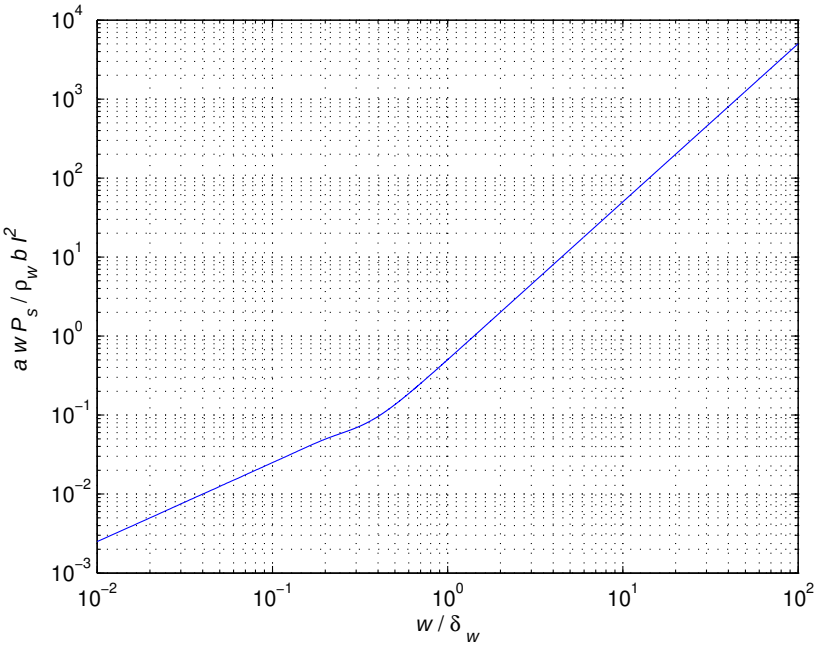

Figure 35: Plot of the power loss due to skin effect $awP_s/b\rho_w I^2$ as a function of w .

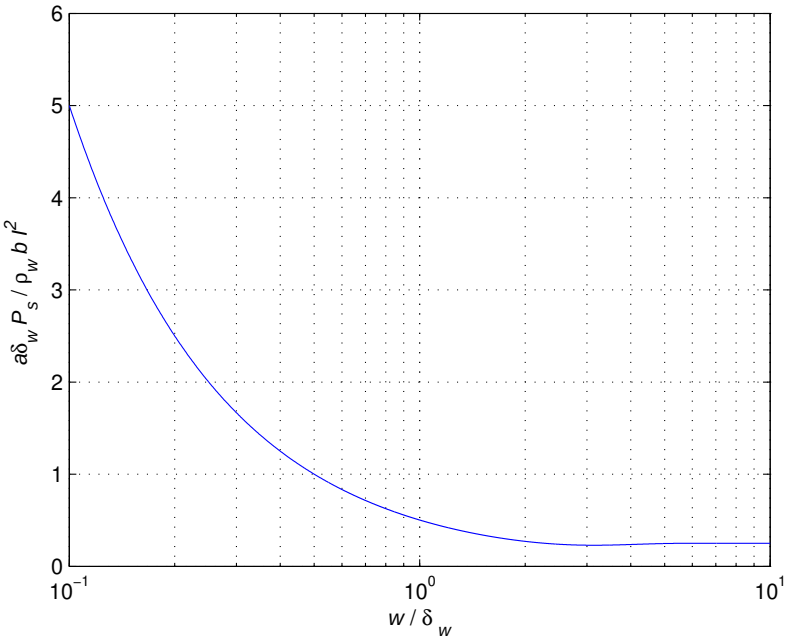

Figure 36: Plot of the power loss due to skin effect $a\delta_w P_s/b\rho_w I^2$ as a function of w/δ_w at fixed δ_w.

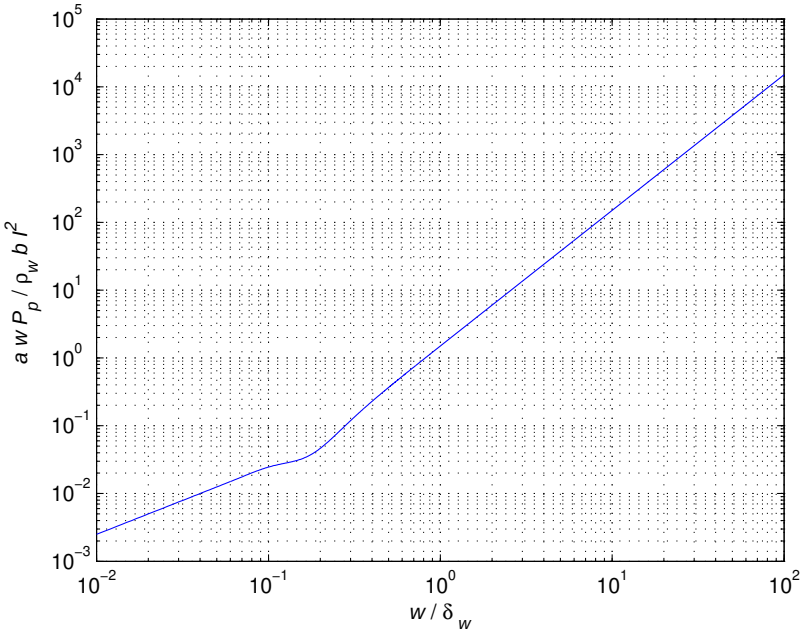

Figure 37: Plot of the power loss due to proximity effect $awP_p/b\rho_w I^2$ as a function of w/δ_w at fixed w.

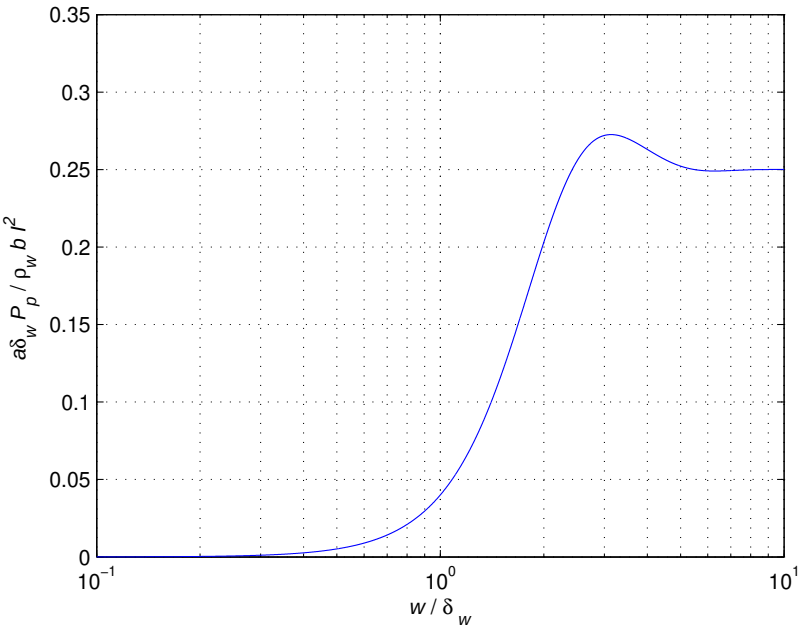

Figure 38: Plot of the power loss due to proximity effect $a\delta_w P_p/b\rho_w I^2$ as a function of w/δ_w at fixed δ_w.

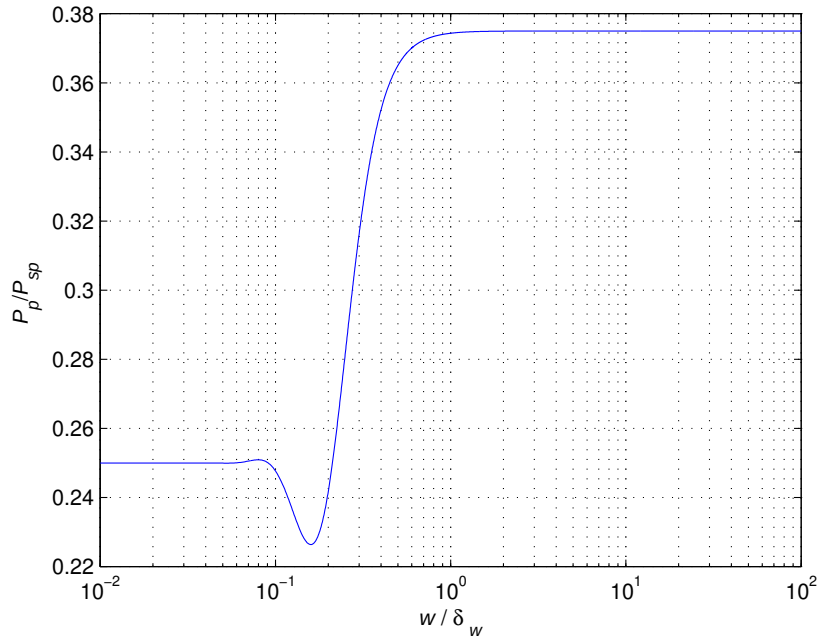

Figure 39: Plot of the ratio P_p/P_{sp} as a function of w/δ_w at fixed w.

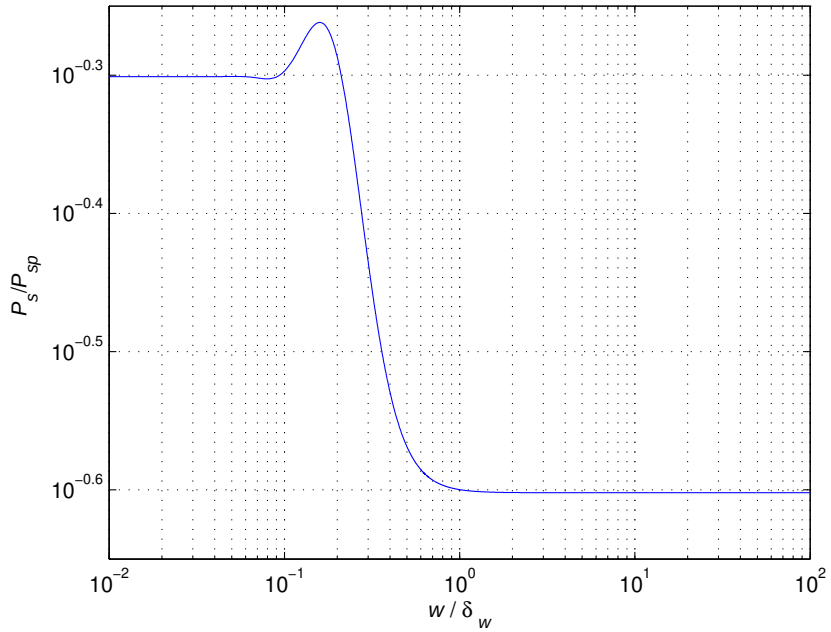

Figure 40: Plot of the ratio P_s/P_{sp} as a function of w/δ_w .

Fig. 35 shows a plot of $awP_s/\rho_w bI^2$ as a function of w/δ_w.The plot shows that when the frequency increases, the power loss due to the skin effect also increases.

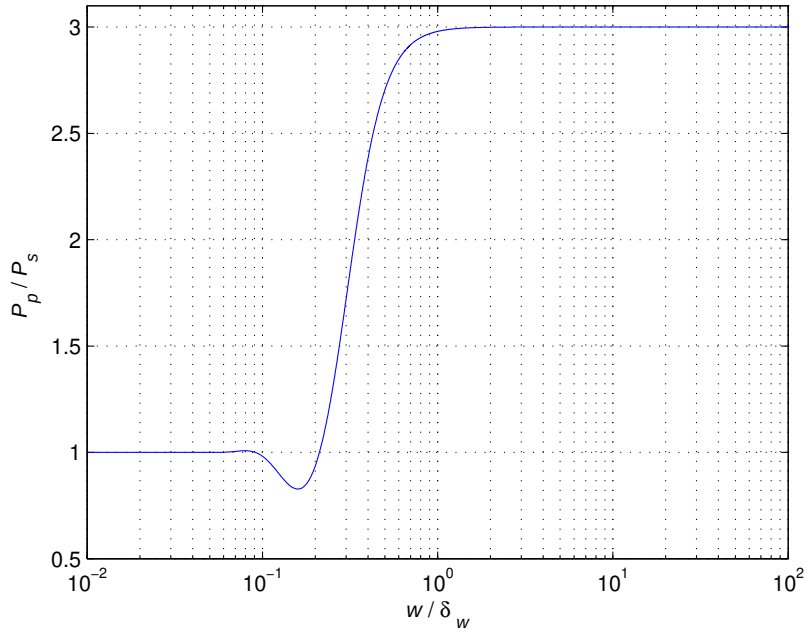

Figure 41: Plot of the ratio P_p/P_s as a function of w/δ_w .

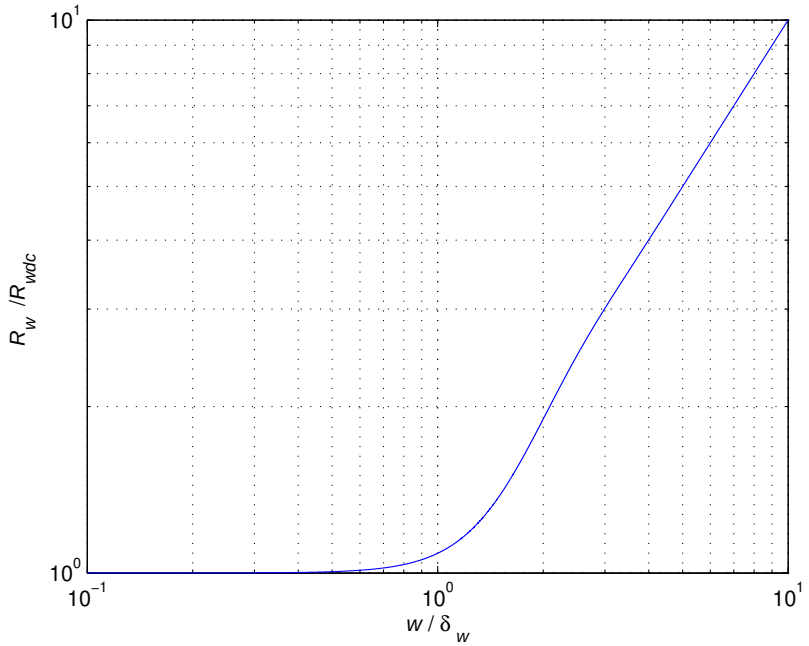

Figure 42: Plot of the ratio R_w/R_{wdc} as a function of w/δ_w .

Fig. 36 shows a plot of $a\delta_w P_s/\rho_w bI^2$ as a function of w/δ_w.The plot shows that when the width of the plate increases, the power loss due to the skin effect decreases.

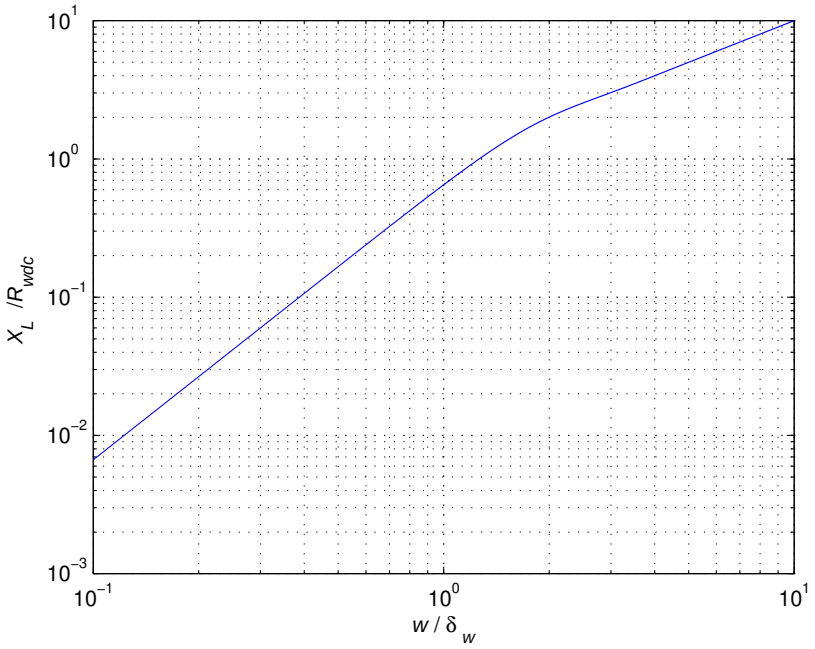

Figure 43: Plot of X_L/R_{wdc} as a function of w/δ_w .

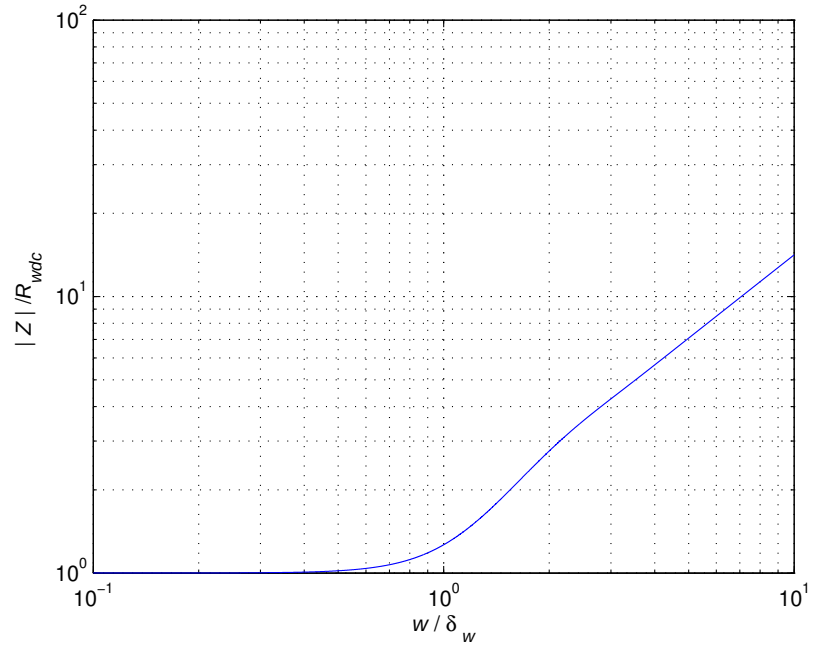

Figure 44: Plot of $|Z|/R_{wdc}$ as a function of w/δ_w .

Fig. 37 shows the power loss due to proximity effect $awP_p/\rho_w bI^2$ as a function of

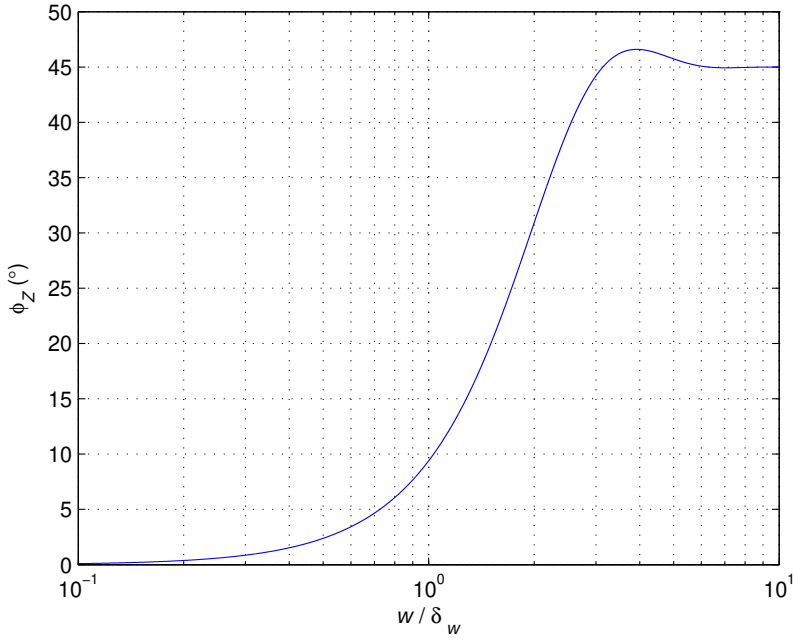

Figure 45: Plot of ϕ_Z as a function of w/δ_w.

w/δ_w.The plot shows that when the frequency increases, the power loss due to the proximity effect also increases.

Fig. 38 shows the power loss due to proximity effect $a\delta_w P_p/\rho_w bI^2$ as a function of w/δ_w.The plot shows that when the width of the plate increases, the power loss due to the proximity effect decreases.

Fig. 39 shows the ratio of P_p/P_{sp} as a function of w/δ_w.

Fig. 40 shows the ratio of P_s/P_{sp} as a function of w/δ_w.

Fig. 41 The ratio of P_p/P_s as a function of w/δ_w.

The power loss in each plate can be expressed as

$$P_{sp} = \frac{1}{2} I^2 R_w = \frac{\rho_w bI^2}{2a\delta_w} \frac{sinh(\frac{2w}{\delta_w}) + sin(\frac{2w}{\delta_w})}{cosh(\frac{2w}{\delta_w}) - cos(\frac{2w}{\delta_w})}. \tag{63}$$

Thus, the normalized resistance of each plate is

$$F_R = \frac{R_w}{R_{wdc}} = (\frac{w}{\delta_w}) \frac{sinh(\frac{2w}{\delta_w}) + sin(\frac{2w}{\delta_w})}{cosh(\frac{2w}{\delta_w}) - cos(\frac{2w}{\delta_w})}. \tag{64}$$

The skin and proximity effects are orthogonal. It can be shown that

$$\int\int_s J_s J_p = 0. \tag{65}$$

The electric field intensity is

$$E = \rho_w J = -\rho_w \frac{dH}{dx} = -\frac{\rho_w \gamma I}{a} \frac{cosh[\gamma(x + \frac{w}{2}]}{sinh(\gamma w)}. \tag{66}$$

The impedance of each plate is

$$Z = \frac{V}{I} = \frac{bE(\frac{w}{2})}{a} cotrh(\gamma w) = R_{wdc}(\frac{w}{\delta_w})(1+j)coth(\gamma w) = F_R + jF_X \tag{67}$$

where

$$F_R = \frac{R_w}{R_{wdc}} = (\frac{w}{\delta_w}) \frac{sinh(\frac{2w}{\delta_w}) + sin(\frac{2w}{\delta_w})}{cosh(\frac{2w}{\delta_w}) - cos(\frac{2w}{\delta_w})}. \tag{68}$$

and

$$F_X = \frac{X_L}{R_{wdc}} = (\frac{w}{\delta_w}) \frac{sinh(\frac{2w}{\delta_w}) - sin(\frac{2w}{\delta_w})}{cosh(\frac{2w}{\delta_w}) - cos(\frac{2w}{\delta_w})}. \tag{69}$$

At high frequencies, the resistance of each plate is

$$F_R = F_X \approx \frac{w}{\delta_w}. \tag{70}$$

Figs. 42 and 43 show plots of R_w/R_{wdc} and X_L/R_{wdc} as a function of w/δ_w.

figs. 44 and 45 show plots of $|Z|/R_{wdc}$ and ϕ_z as a function of w/δ_w.

5 Anti-proximity and Skin Effects in Two Parallel Plates

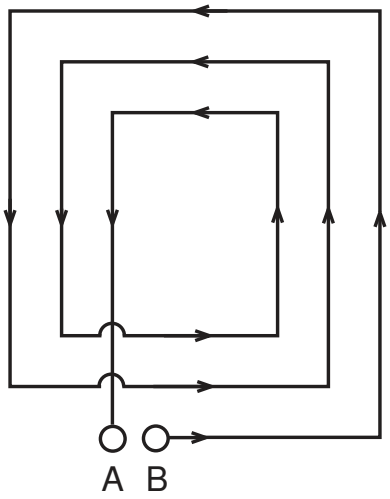

Figure 46: Typical pattern of multi-layer inductor winding.

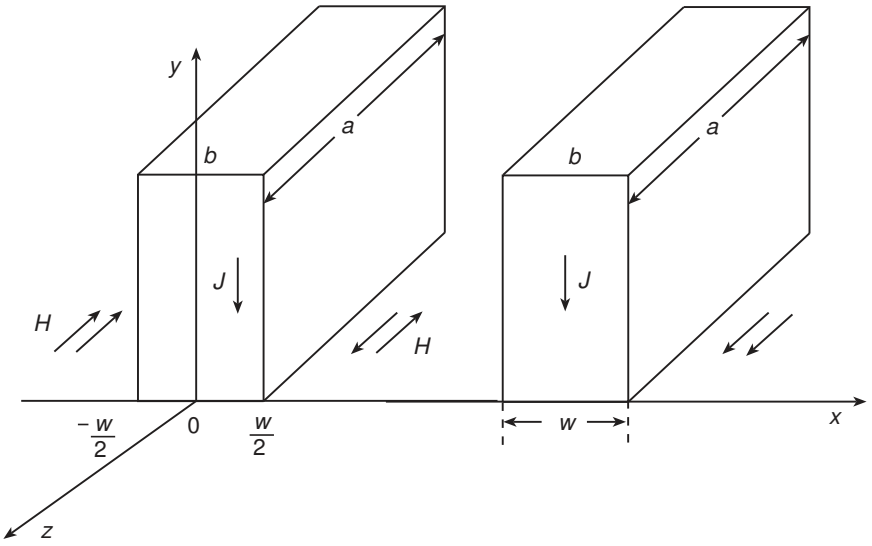

Figure 47: Two plates carrying currents in the same directions.

A typical pattern of inductor winding is shown in Fig.46. It can be seen that the current flows in the same direction in the adjacent layers. Fig. 47 shows two rectangular parallel conducting plates. Consider the case in which the current $i(t) = Icoswt$ flow in the plate in the same direction. Both currents flow in the $-y$ direction.

The current induce the magnetic field in side and out side the plates. the magnetic fields generated by both plates subtract from each other between the plates and add to each other out side the plates, causing larger current density $J(x)$ in the plate areas, where the plates are far from each other. The magnetic field is described by the Helmholtz equation

$$\frac{d^2H(x)}{dx^2} = \gamma^2 H(x). \tag{71}$$

A general solution of this equation is

$$H(x) = H_1 e^{\gamma x} + H_2 e^{-\gamma x}. \tag{72}$$

where

$$H_1 = \frac{I}{a}\frac{e^{\gamma\frac{w}{2}}}{e^{\gamma w} + e^{-\gamma w}}. \tag{73}$$

and

$$H_2 = -\frac{I}{a}\frac{e^{-\gamma\frac{w}{2}}}{e^{\gamma w} + e^{-\gamma w}}. \tag{74}$$

The magnetic field is given by

$$H(x) = \frac{I}{a}\frac{sinh[\gamma(x - \frac{w}{2})]}{sinh(\gamma w)}. \tag{75}$$

Fig. 48, 49 and 50 show plots of $a|(Hx)|/I$ and its real and imaginary parts as a function of x/w for selection values of w/δ_w.

The current density is

$$J(x) = -\frac{dH(x)}{dx} = -\frac{\gamma I}{a}\frac{cosh[\gamma(x - \frac{w}{2})]}{sinh(\gamma w)}. \tag{76}$$

Fig. 51, 52 and 53 show plots of $a|(Jx)|/I$ and its real and imaginary parts as a function of x/w for selection values of w/δ_w.

The current density due to the skin and proximity on effects on the surfaces of the conductor for $x = w/2$ and $x = -w/2$ is given by

$$J_{sp}(\frac{w}{2}) = -\frac{\gamma I}{a}\frac{cosh(\gamma\frac{w}{2})}{sinh(\gamma w)}. \tag{77}$$

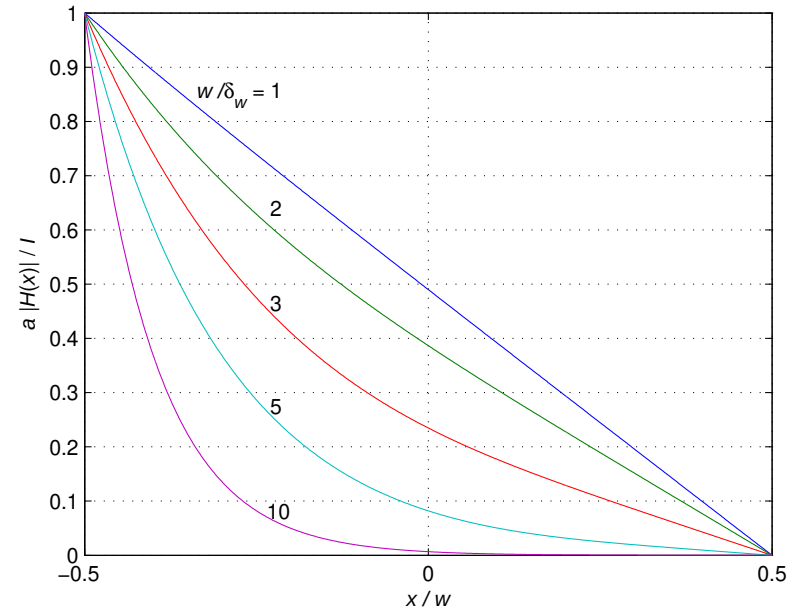

Figure 48: Plot of $a|H(x)|/I$ as a function of x/w for selected values of w/δ_w in the left plate due to the proximity effect.

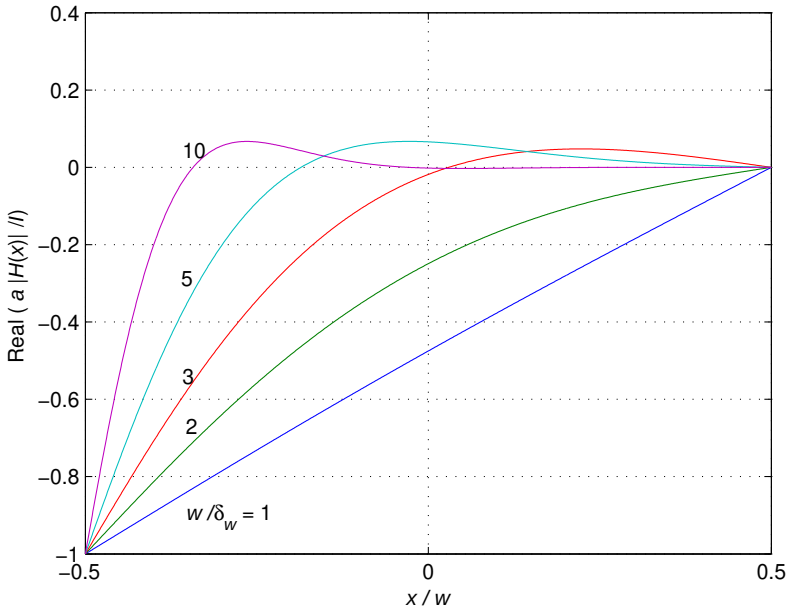

Figure 49: Plot of the real part of $a|H(x)|/I$ as a function of x/w for selected values of w/δ_w. The current density is given by in the left plate due to the proximity effect.

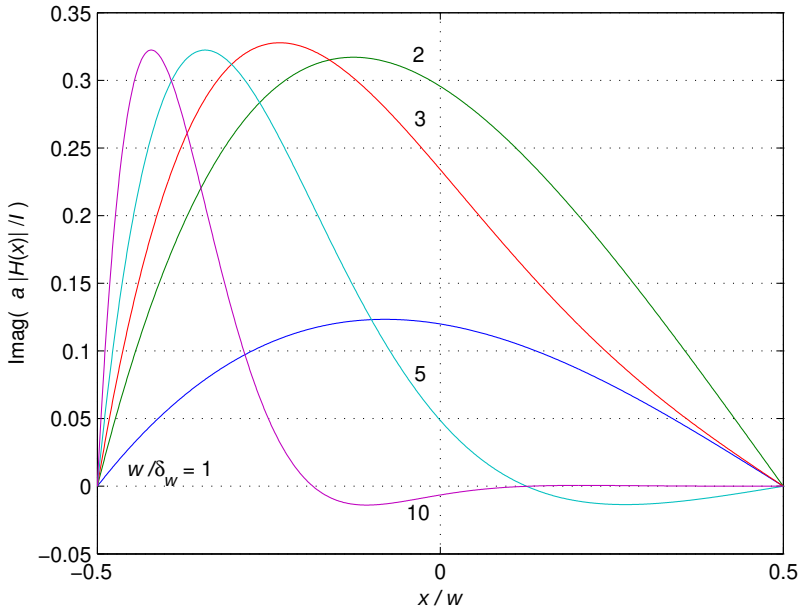

Figure 50: Plot of the imaginary part of $a|H(x)|/I$ as a function of x/w for selected values of w/δ_w. The current density is given by in the left plate due to the proximity effect.

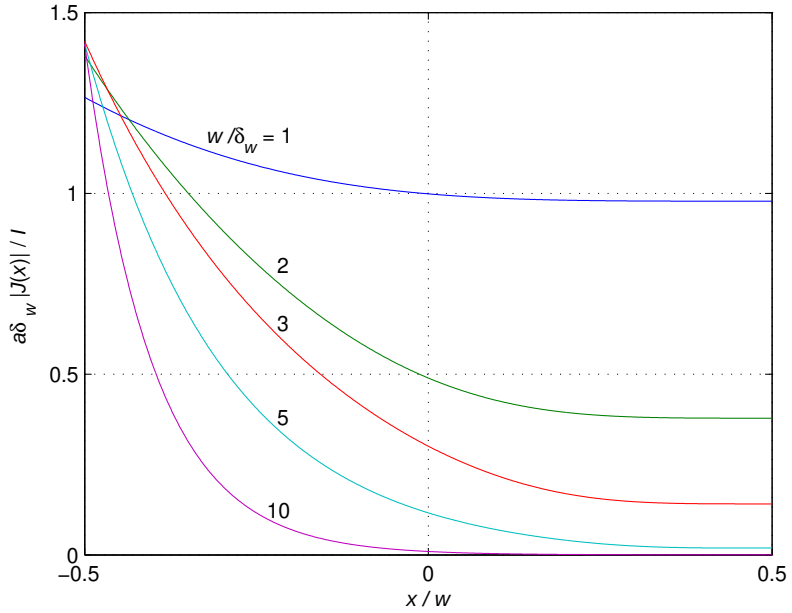

Figure 51: Plot of $a|J(x)|/I$ as a function of x/w for selected values of w/δ_w in the left plate due to the proximity effect.

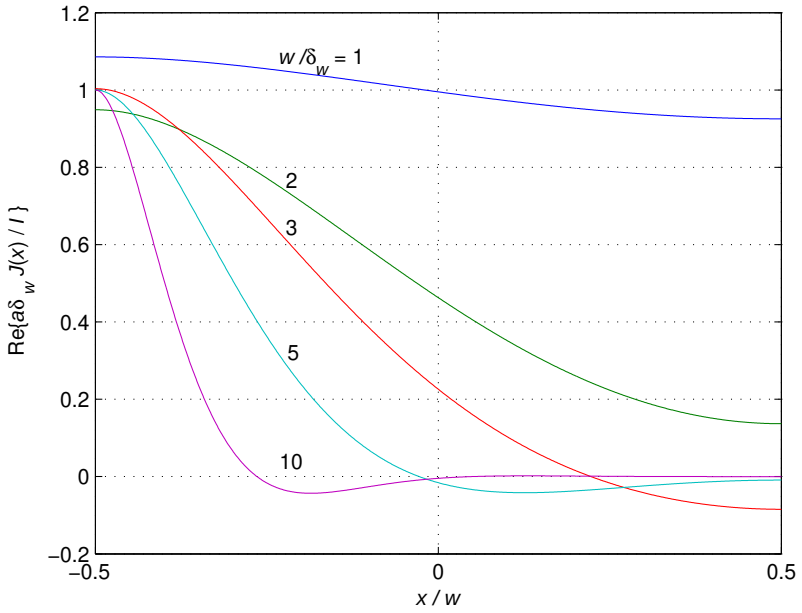

Figure 52: Plot of the real part of $a|J(x)|/I$ as a function of x/w for seleced values of w/δ_w. The current density is given by in the left plate due to the proximity effect.

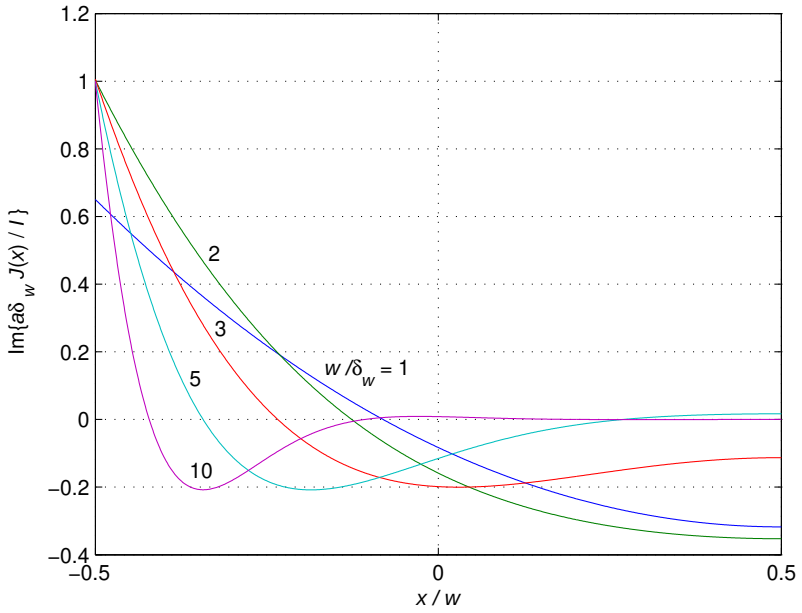

Figure 53: Plot of the imaginary part of $a|J(x)|/I$ as a functed of x/w for selection values of w/δ_w. The current density is given by in the left plate due to the proximity effect.

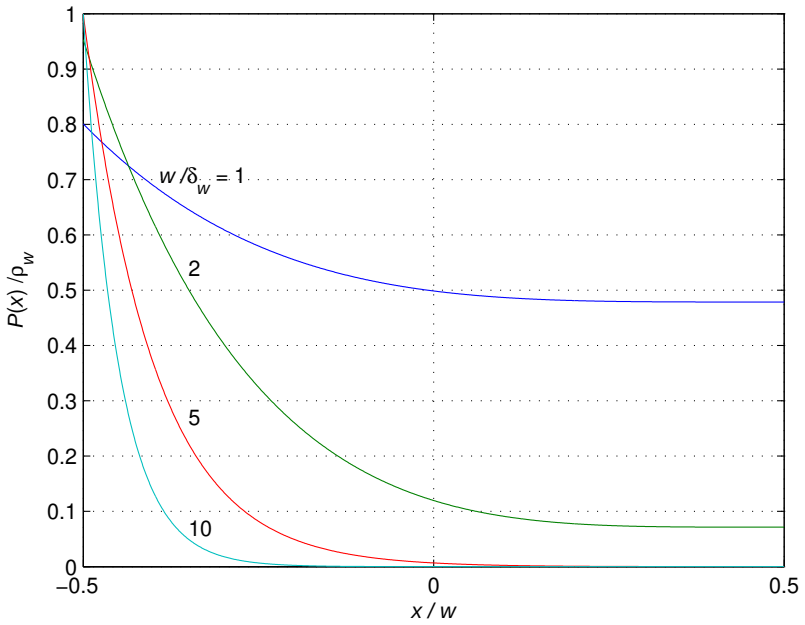

Figure 54: Plot of $P(x)/\rho_w$ as a function of x/w for selected values of w/δ_w in the left plate due to the proximity effect.

and

$$J_{sp}(-\frac{w}{2}) = -\frac{\gamma I}{a}\frac{1}{sinh(\gamma w)}. \tag{78}$$

hence,

$$\frac{J_{sp}(-\frac{w}{2})}{J_s(-\frac{w}{2})} = \frac{1}{1+sinh^2(\gamma\frac{w}{2})} \tag{79}$$

$$\frac{J_{sp}(\frac{w}{2})}{J_s(\frac{w}{2})} = 1+tanh^2(\gamma\frac{w}{2}) \tag{80}$$

and

$$\frac{J_{sp}(0)}{J_s(0)} = 1. \tag{81}$$

The local power density is

$$P(x) = \frac{1}{2}\rho_w|J(x)|^2. \tag{82}$$

Fig. 54 shows plots of $P(x)/\rho_w$ as a function of x/w for selection values of w/δ_w in the left plate due to the proximity effect.

The total power loss in each conductor due to the proximity and skin effects is

$$P_{sp} = \frac{\rho_w b I^2}{2a\delta_w} \frac{sinh(\frac{2w}{\delta_w}) + sin(\frac{2w}{\delta_w})}{cosh(\frac{2w}{\delta_w}) - cos(\frac{2w}{\delta_w})}. \tag{83}$$

Comparing the power loss in a single conductor and two conductors, we can see that the presence of second conductor has increased the loss in the first. this increase is simply the proximity loss set up in the first conductor by the magnetic field of the second.

The proximity loss is

$$P_p = \frac{\rho_w b I^2}{4a\delta_w} \frac{sinh(\frac{2w}{\delta_w}) - sin(\frac{2w}{\delta_w})}{cosh(\frac{2w}{\delta_w}) + cos(\frac{2w}{\delta_w})}. \tag{84}$$

hence

$$P_s = P_{sp} - P_p = \frac{\rho_w b I^2}{4a\delta_w} \frac{sinh(\frac{2w}{\delta_w}) + sin(\frac{2w}{\delta_w})}{cosh(\frac{2w}{\delta_w}) - cos(\frac{2w}{\delta_w})}. \tag{85}$$

6 Laminated Cores

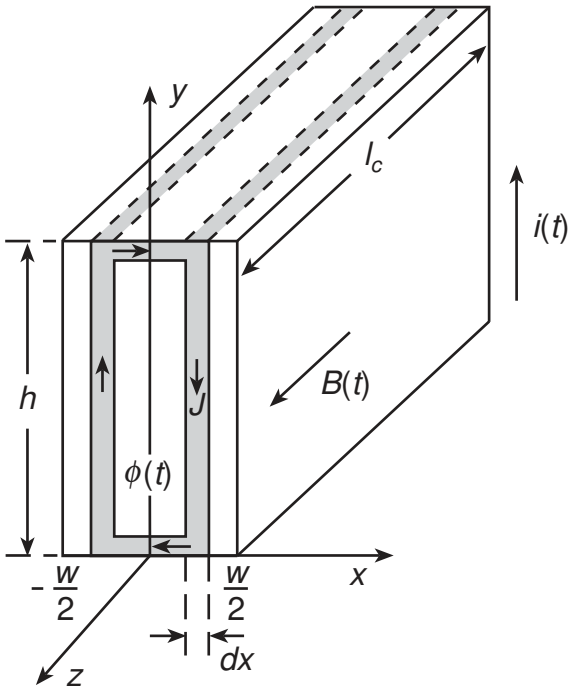

Figure 55: Cross section of single lamination used to analyzing eddy-current loss.

As previously discussed in Chapter 2, there are two kinds of eddy-currents. One occurs due to the skin effect and the other occurs due to the proximity effect. In this chapter, the method for the reduction of these two kinds of eddy-current loss will be discussed. The first method is by using a high-resistivity material for the cores. This high-resistivity increases the skin depth δ_c, and , thus reduces w/δ_c, that makes the distribution of the magnetic flux density B more uniform. If this happens, the condition $w/\delta_c < 1$ is satisfied over a wider frequency range. In order to increase the core resistivity ρ_c and therefore reduce the eddy-current amplitude, the iron is used with a small amount of silicon or chrome (1 to 5%), producing a magnetic steel. Ferrite and powder cores are also example of material with high resistivity. The second method to reduce the eddy-current that occurs due to proximity effect is to divide the core in to large number of thin slices that are insulated from each other using

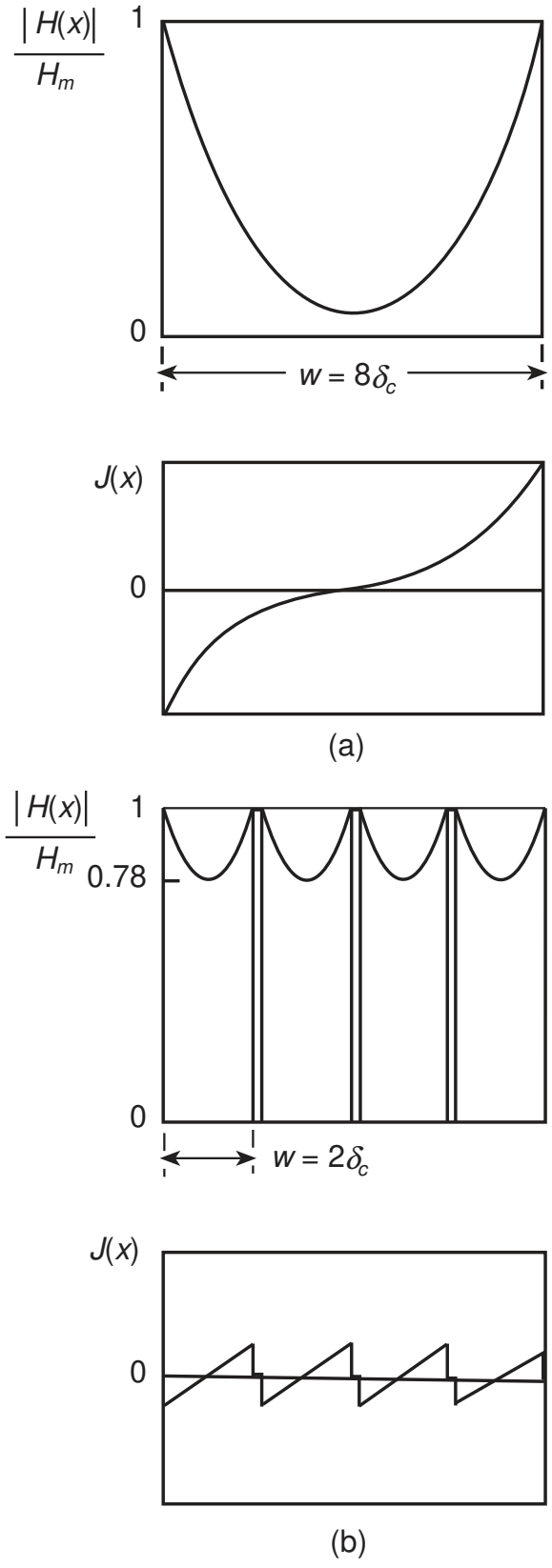

Figure 56: Distribution of the envelope of the amplitude of magnetic field intensity $H(x)/H_m$ and the eddy density $J(x)$. (a) For a single solid core at $w = 8\delta_c$. (b) For laminated core at $w/2\delta_c$.

oxide film. This thin insulated sheet called lamination, are oriented parallel to the magnetic flux ϕ. Thin laminations have little flux in individual layers and therefore, the induced voltage decreases. Also the resistance of a single lamination is k times higher than that of the corresponding solid core, where k is the number of sheets. Laminations are insulated from each other by an oxide film or insulated varnish and then stacked together to form the magnetic core. If thin sheets are used then, more of core volume is needed. The lamination thickness w ranges from 0.01 to .5 mm. The typical thickness usually is 0.3 mm for frequencies up to 200 Hz, 0.1 mm for frequencies between 200 Hz and 2 kHz, and 0.05 mm for higher frequencies and pules applications. The typical thickness of insulation is 0.015 mm. The most common core use 97 % iron and 3 % silicon. They have μ_r = 10,000 and lamination thickness equal to 0.3 mm. In powder core, eddy-current loss is low because individual particles are insulated from each other. Laminations do not affect the magnetic performance of the core at low frequencies. Line frequency transformers and electric machines use laminated cores.

The other reason for using lamination is the skin effect. Otherwise, a solid core would contain flux only in a shell with thickness equal to the core skin depth δ_c. As w/δ_c is increased from 1 to 10, $H(0)/H(w/2)$ and $B(0)/B(w/2)$ decrease from approximately 1 to 10. For example.$B(0)/B(w/2) = 0.98$ at $w/\delta_c = 1$, $B(0)/B(w/2) = 0.78$ at $w/\delta_c = 2$, $B(0)/B(w/2) = 0.46$ at $w/\delta_c = 3$, and $B(0)/B(w/2) = 0.1$ at $w/\delta_c = 8$. When the core resistivity ρ_c is increased, the core skin depth δ_c also increased. Therefore, there will be low frequency range, in which $\delta_c > w$, the distribution of H is nearly uniform, and the skin effect in the core can be neglected.

6.1 Low-Frequency Solution

The derivation of the eddy-current power loss in lamination iron for low frequencies (where $\delta_c >> w$) is as follows. The eddy-current density is assumed to be uniform.

Consider an iron lamination without an air gap, shown in Fig. 7. Assumed that $h >> w$ and $\delta_c > w$, let us assume that the distribution of H along the $x-$axis is uniform. Also, assume that a sinusoidal current flows in the inductor winding

$$i(t) = I_m sin\omega t. \tag{86}$$

resulting in the magnetic flux density in the core

$$B(t) = B_m sin\omega t. \tag{87}$$

The distribution of the magnetic flux $B = B_z$ in the core is uniform for $w < \delta_c$. The area through which the magnetic flux is passing for $x > 0$ is given by

$$A_\phi = hx \quad \text{for} \quad x > 0. \tag{88}$$

and the magnetic flux passing through half of the area encircled by eddy-current loop is

$$\phi_t = A_\phi B_m sin\omega t = hxB_M sin\omega t \quad \text{for} \quad x > 0. \tag{89}$$

By Faraday's low, the voltage induced between the bottom and top terminals is equal to the derivative of the magnetic flux passing through half of the area enclosed by the eddy-current loop

$$v(t) = \frac{d\phi(t)}{dt} = A_\phi \frac{dB(x)}{dt} = hxwB_m cos\omega t = A_\phi wB_m cos\omega t = V_m coswt \tag{90}$$

where

$$V_m = \omega B_m hx. \tag{91}$$

Thus, V_m is proportional to f, B_m, h and x. By Lenz's law, the voltage $v(t)$ induces the eddy-currents J, which, in turn, generate flux $\phi'(t)$ that tend to oppose the imposed flux $\phi(t)$. Since V_m increases with x, the maximum current density in the middle of the lamination.

The lamination resistance of thickness x and area$A_{ex} = xl_c$ is

$$R_{cx} = \rho_C \frac{h}{A_{ex}} = \rho_c \frac{h}{l_c x} \tag{92}$$

resulting in the amplitude of the eddy-current

$$I_{em} = \frac{V_m}{R_{cx}} = \frac{\omega B_m l_c x^2}{\rho_c} \tag{93}$$

and in the eddy-current density

$$|J_m(x)| = \frac{I_{em}}{A_{ex}} = \frac{\omega B_m x}{\rho_c}. \tag{94}$$

It can be seen that the amplitude of the eddy current density change linearly with the distance x. It is zero in the middle of the lamination and increases with the distance x from the middle of the lamination. The maximum amplitude of eddy-current density is at the surface

$$J_{m(max)} = J_m(\frac{w}{2}) = \frac{\omega B_m w}{2\rho_c}. \tag{95}$$

The time-average eddy-current power loss in the lamination at low frequencies is

$$P_E = \int\int\int_{v_c} \frac{\rho_c J_m^2(x)}{2} dxdydz = \frac{\rho_c}{2} \int_0^{l_c} \int_0^h \int_{-\frac{w}{2}}^{\frac{w}{2}} \frac{\omega^2 B_m^2 x^2}{\rho_c^2} dxdydz$$

$$= \rho_c \int_0^{l_c} \int_0^h \int_0^{\frac{w}{2}} \frac{\omega^2 B_m^2 x^2}{\rho_c^2} dx = \frac{\pi^2 f^2 B_m^2 h l_c w^3}{6\rho_c} \quad \text{for} \quad w < \rho_c. \tag{96}$$

yielding the time-averaged eddy-current power loss per unit volume (or the specific eddy-current power loss) at sinusoidal waveform of $B(t) = B_m sinwt$

$$P_e = \frac{P_E}{V_c} = \frac{\pi^2 f^2 w^2 B_m^2}{6\rho_c} = \frac{\omega^2 w^2 B_m^2}{24\rho_c} \quad \text{for} \quad w < \delta_c = \sqrt{\frac{\rho_c}{\pi \mu_{rc} \mu_0 f}}. \tag{97}$$

where $V_c = whl_c$ is the single lamination volume and w the single lamination thickness. Note that P_E is proportional to w^3 and P_e is proportional to w^2. It is evident from the above expression that the eddy-current power loss density at low frequencies is reduced by using thinner laminations and core material with high resistivity.

An alternative method of deriving an expression for P_E is as follows. The resistance of a thin strip with eddy-current is

$$R = \rho_c \frac{h}{l_c dx}. \tag{98}$$

Hence, the eddy-current power dissipated in the thin lamination is

$$dP_E = \frac{V_m^2}{2R} = \frac{hl_c\omega^2 B_m^2}{2\rho_c}x^2 dx \tag{99}$$

resulting in the eddy-current power dissipated in lamination at low frequencies

$$P_E = \int_{-\frac{w}{2}}^{\frac{w}{2}} dP_E = 2\int_0^{\frac{w}{2}} dP_E = \frac{hl_c\omega^2 B_m^2}{\rho_c}\int_0^{\frac{w}{2}} x^2 dx = \frac{hl_c w^3\omega^2 B_m^2}{24\rho_c}$$
$$= \frac{w^2\omega^2 B_m^2}{24\rho_c}V_c = \frac{\pi^2 f^2 w^2 B_m^2}{6\rho_c}V_c \quad \text{for} \quad w < \delta_c. \tag{100}$$

From the equation, the loss due to eddy-current is proportional to the square of the frequency and the cube of the thickness.

Let's assume that a solid core width is $w_s = kw$, the ratio of the eddy-current power loss density in sold core P_{es} to that in the single lamination P_e is

$$\frac{P_{es}}{P_e} = (\frac{w_s}{w})^2 = k^2 \quad \text{for} \quad w < \delta_c = \sqrt{\frac{\rho_c}{\pi\mu_{rc}\mu_0 f}}. \tag{101}$$

The ratio the eddy-current power loss in a sold core P_{Es} to the eddy-current power loss that in the lamination core consisting of k laminations P_{El} is

$$\frac{P_{Es}}{P_E} = (\frac{w_s}{w})^3 = k^3 \quad \text{for} \quad w < \delta_c = \sqrt{\frac{\rho_c}{\pi\mu_{rc}\mu_0 f}}. \tag{102}$$

Now, the ratio of the eddy-power loss in a solid core P_{Es} that in the single lamination P_e is

$$\frac{P_{Es}}{P_{El}} = \frac{P_{Es}}{kP_E} = (\frac{w_s}{w})^2 = k^2 \quad \text{for} \quad w < \delta_c = \sqrt{\frac{\rho_c}{\pi\mu_{rc}\mu_0 f}}. \tag{103}$$

Therefore, the eddy-current power loss in the sold core k^2 time higher than in that in the lamination core, assuming that both core have the same conducting volume.

The solid core resistance at low frequencies is

$$R_{csd} = \rho_c\frac{h}{A_{cs}} = \rho_c\frac{h}{w_s l_c}. \tag{104}$$

The resistance of a single lamination is

$$R_{csl} = \rho_c\frac{h}{A_{cs}} = \rho_c\frac{h}{w_s l_c} = kR_{csd}. \tag{105}$$

The core resistance of the laminated core with k laminations at low frequencies is

$$R_{cl} = \rho_c \frac{h}{kwl_c} = R_{csd}. \tag{106}$$

6.2 General Solution

At any frequency, the magnetic field intensity is described by the Helmholtz equation

$$\frac{d^2H_z(x)}{dx^2} = \gamma^2 H_z(x) = j\mu_c\omega H_z(x) \tag{107}$$

where

$$\gamma = \sqrt{j\mu_c\sigma_c\omega} = (1+j)\sqrt{\mu_c\sigma_c f} = \frac{1+j}{\delta_c} \tag{108}$$

with the depth into the conductor sheet given by

$$\delta_c = \frac{1}{\sqrt{\pi\mu_c\sigma_c f}} = \sqrt{\frac{\rho_c}{\pi\mu_c f}}. \tag{109}$$

A general solution of (107) is

$$H(x) = H_1 e^{\gamma x} + H_2 e^{-\gamma x}. \tag{110}$$

Hence,

$$H(\frac{w}{2}) = H_1 e^{\gamma\frac{w}{2}} + H_2 e^{-\gamma\frac{w}{2}} \tag{111}$$

and

$$H(-\frac{w}{2}) = H_1 e^{-\gamma\frac{w}{2}} + H_2 e^{\gamma\frac{w}{2}}. \tag{112}$$

The condition of even symmetry requires that $H(x) = H(-x)$, from which $H(w/2) = H(w/2)$.

Subtract (112) from (111), we get

$$H(\frac{w}{2}) - H(-\frac{w}{2}) = H_1 e^{\gamma\frac{w}{2}} + H_2 e^{-\gamma\frac{w}{2}} - H_1 e^{-\gamma\frac{w}{2}} - H_2 e^{\gamma\frac{w}{2}} = (e^{\gamma\frac{w}{2}} + e^{-\gamma\frac{w}{2}})(H_1 - H_2) = 0 \tag{113}$$

from

$$H_1 = H_2. \tag{114}$$

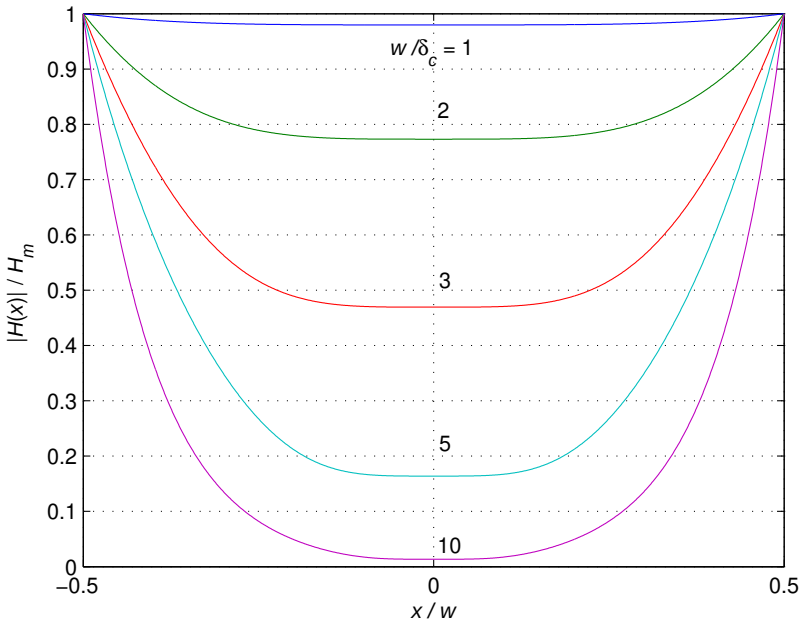

Figure 57: Plot of $|H(x)|/H_m$ as a function of x/w for selected values of w/δ_c.

Substituting for H_2 in (110), we get

$$H(x) = H_1(e^{\gamma x} + e^{-\gamma x}) = 2H_1\frac{e^{\gamma x} + e^{-\gamma x}}{2} = 2H_1 cosh(\gamma x). \tag{115}$$

Using the boundary condition,

$$H(\frac{w}{2}) = 2H_1 cosh(\frac{\gamma w}{2}) \tag{116}$$

we obtain

$$H_1 = \frac{H(\frac{w}{2})}{2cosh(\frac{\gamma w}{2})} \tag{117}$$

the amplitude of the magnetic field intensity at $x = w/2$ is

$$H(\frac{w}{2}) = H_m = \frac{NI_m}{l_c}. \tag{118}$$

Substitute (117) and (118) into (115), we get the solution of the Helmholtz equation

$$H(x) = H_m\frac{cosh(\gamma x)}{cosh(\gamma\frac{w}{2})} = H_m\frac{cosh(\frac{x}{\delta_c} + j\frac{x}{\delta_c})}{cosh(\frac{x}{2\delta_c} + j\frac{x}{2\delta_c})} = H_m\frac{cosh[(1+j)(\frac{w}{\delta_c})(\frac{x}{w})]}{cosh[\frac{(1+j)}{2}(\frac{w}{\delta_c})]}. \tag{119}$$

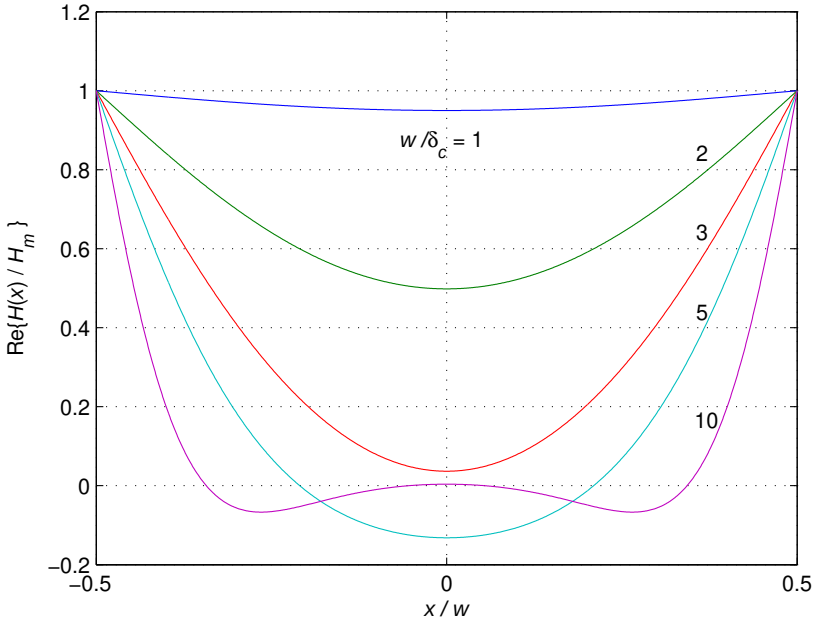

Figure 58: The real part of $|H(x)|/H_m$ as a function of x/w for selected values of w/δ_c.

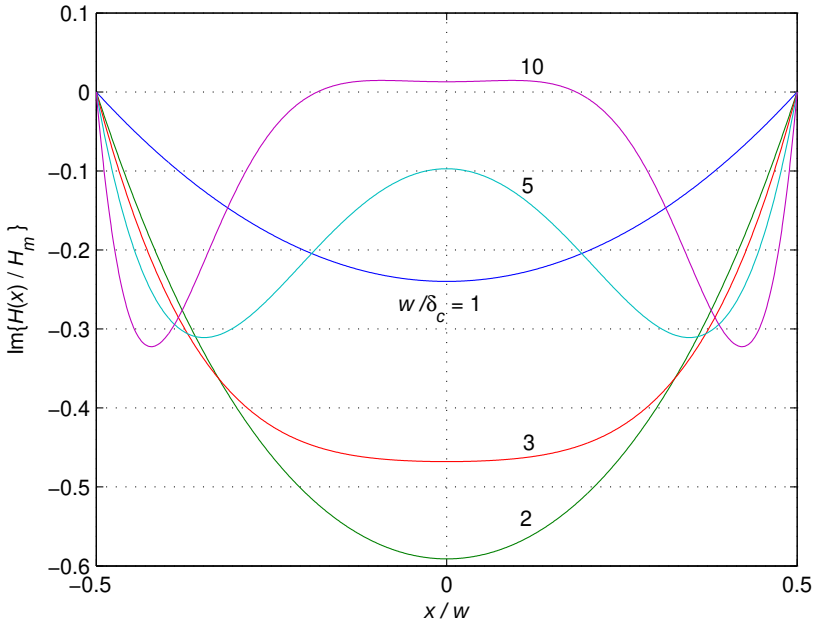

Figure 59: The imaginary part of $|H(x)|/H_m$ as a functed of x/w for selected values of w/δ_c.

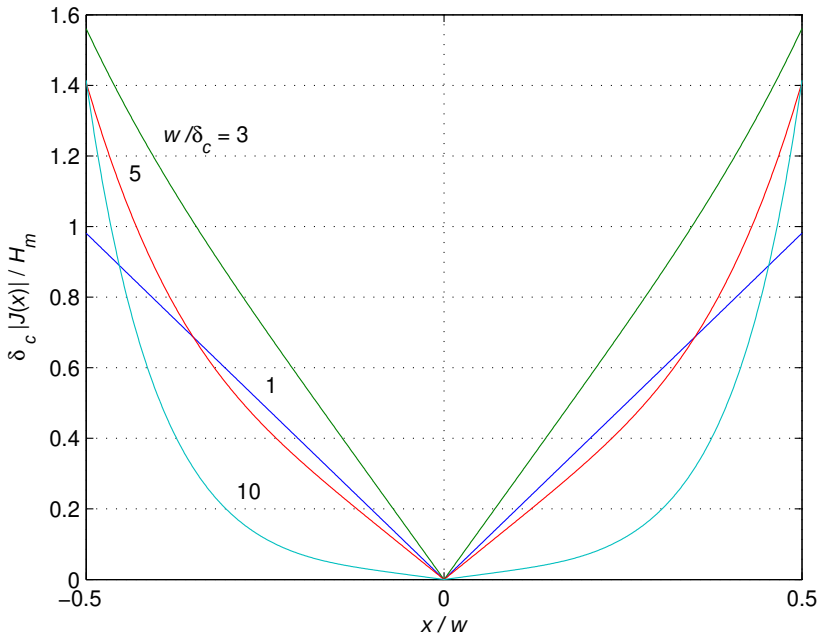

Figure 60: Plot of $\delta_c|J(x)|/H_m$ as a function of x/w for selected values of w/δ_c.

The magnitude of the magnetic field intensity is

$$|H(x)| = H_m\sqrt{\frac{cosh^2\frac{x}{\delta_c} - sin^2\frac{x}{\delta_c}}{cosh^2\frac{w}{2\delta_c} - sin^2\frac{w}{2\delta_c}}} = H_m\sqrt{\frac{cosh\frac{2x}{\delta_c} + cos\frac{2x}{\delta_c}}{cosh\frac{w}{\delta_c} + sin\frac{w}{\delta_c}}}. \quad (120)$$

Fig. 57 ,58 and 59 show plots of $H(x)/H_m$ and its real and imaginary parts as a function of x/w at different values of w/δ_c.

The current density is

$$J(x) = J_y(x) = -\frac{dH_z(x)}{dx} = -\gamma H_m\frac{sinh(\gamma x)}{cosh(\gamma\frac{w}{2})} = -\frac{1+j}{\delta_c}H_m\frac{sinh(\frac{x}{\delta_c} + j\frac{x}{\delta_c})}{cosh(\frac{x}{2\delta_c} + j\frac{x}{2\delta_c})}. \quad (121)$$

The magnitude of the current density is

$$|J(x)| = \frac{H_m}{\delta_c}\sqrt{\frac{2[cosh\frac{2x}{\delta_c} - cos\frac{2x}{\delta_c}]}{cosh\frac{w}{\delta_c} + cos\frac{w}{\delta_c}}}. \quad (122)$$

Figs. 60 show plot of $\delta_c|J(x)|/H_m$ as a function of x/w at different values of w/δ_c.

At high frequencies, $\delta_c << w$, the distribution of the envelope of magnetic field intensity $H(x)$ is not uniform and the amplitude of eddy-current density $J(x)$ does

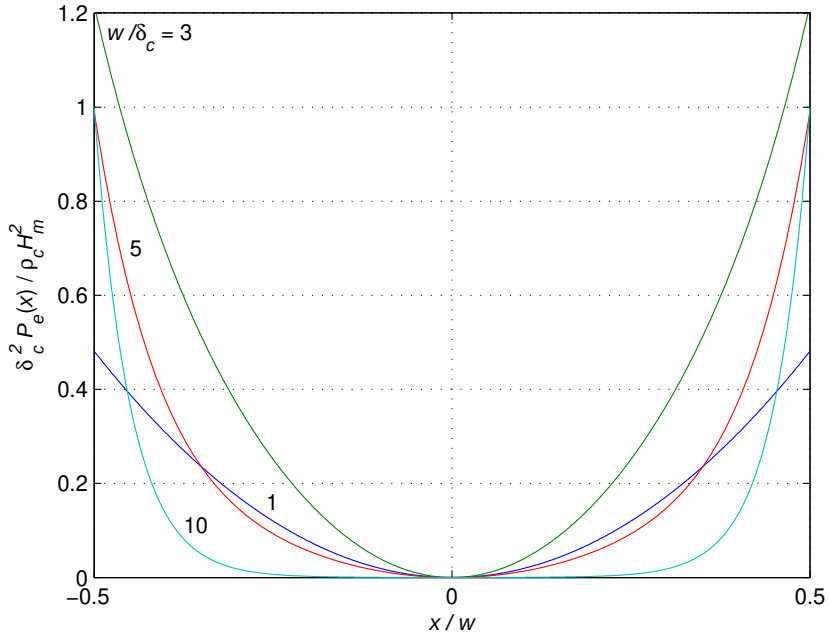

Figure 61: Plot of $\delta_c^2 P_e(x/\rho_c H_m^2)$ as a function of x/w for selected values of w/δ_c.

not vary linearly with distance x, as illustrated in Fig. 56 for a solid core at $w = 8\delta_c$. In this case, $J(w/2)$ is very high, resulting in high core loss. the distribution of $H(x)/H_o$ and $J(x)$ in the laminated core at $w = 2\delta_c$ are depicted in Fig.56 (b). Silicon is often added to steel to reduce σ_c, and reduce w/δ_c, making $H(x)$ more uniform.

Using Ohm's law $\mathbf{E} = \sigma_c \mathbf{J}$, we obtain the time-average eddy-current power loss density

$$P_e(x) = \frac{1}{2}\mathbf{E}\cdot\mathbf{J}^* = \frac{\rho_c}{2}\mathbf{J}\cdot\mathbf{J}^* = \frac{\rho_c |J(x)|^2}{2} = \frac{\rho_c H_m^2}{\delta_c^2}\frac{cosh\frac{2x}{\delta_c} - cos\frac{2x}{\delta_c}}{cosh\frac{w}{\delta_c} + cos\frac{w}{\delta_c}} \tag{123}$$

Fig. 61 shows plot of $\delta_c^2 P_e(x/\rho_c H_m^2)$ as a function of x/w at different values of w/δ_w. Since $sinh(x/\delta_c + jx/\delta_c) \approx (1+j)x/\delta_c$ and $cosh(w/\delta_c + jw/\delta_c) \approx 1$ for $w/delta_c << 1$ and $x/\delta_c << 1$, the current density at law frequencies is approximated by

$$J(x) = J_y(x) \approx H_m \left(\frac{1+j}{\delta_c}\right)^2 x = \frac{B_m}{\mu_c}\left(\frac{1+j}{\delta_c}\right)^2 x = \frac{2B_m}{\mu_c \delta_c^2} x. \tag{124}$$

The complex power for sinusoidal waveforms in phasor form is

$$S_{E(complex)} = \frac{1}{2}\int\int\int_v \mathbf{E}\cdot\mathbf{J}^* dV. \tag{125}$$

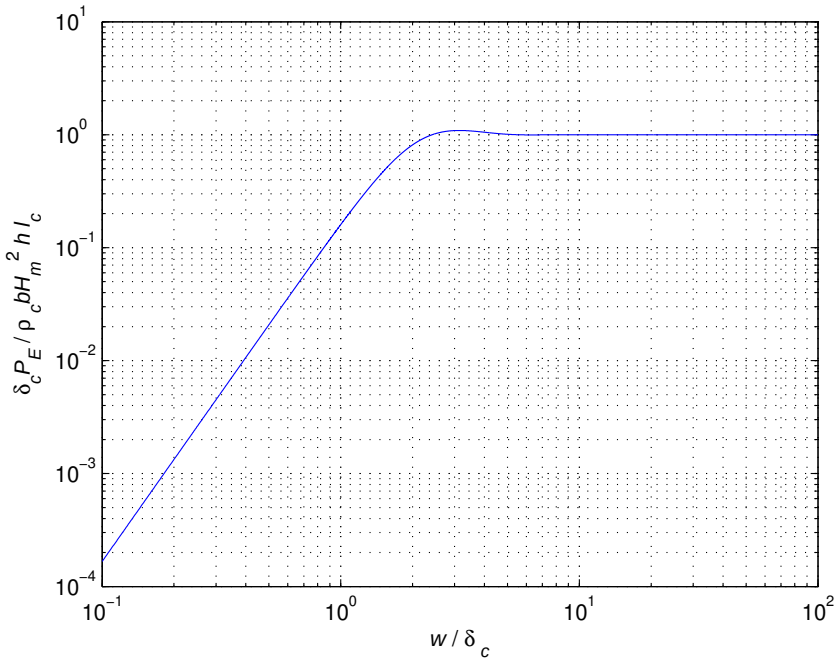

Figure 62: Plot of $\delta_c P_E \rho_c H_m^2 h l_c$ as a function of w/δ_w.

The time-average power dissipated at low frequencies ($w << \delta_c$) is given by

$$P_e = \frac{1}{2} Re\left\{\int\int\int_v \mathbf{E}\cdot\mathbf{J}^* dV\right\} = \frac{1}{2}\int\int\int_v \rho_c |J|^2 dV = \frac{\rho_c}{2}\int\int\int_v |J|^2 dV$$

$$\approx \frac{\rho_c B_m^2}{2\mu_c^2}\int_0^{l_c}\int_0^h \int_{-\frac{w}{2}}^{\frac{w}{2}} \left|\left(\frac{1+j}{\delta_c}\right)x\right|^2 dxdydz$$

$$= \frac{4\rho_c B_m^2}{2\mu_c^2\delta_c^4}\int_0^{l_c}\int_0^h\int_{-\frac{w}{2}}^{\frac{w}{2}} x^2 dxdydz = \frac{\mu_c l_c h w_3 B_c^2}{6\mu_c^2\delta_c^2} = \frac{l_c h w^3 \omega^2 B_m^2}{24\rho_c}. \qquad (126)$$

this expression is identical to that given by (97).

using 119, the time-average eddy-current power loss dissipated in the lamination is

$$P_E = \frac{1}{2}\int\int\int_v \rho_c |J(x)|^2 dV = \frac{1}{2}\int_0^{l_c}\int_0^h\int_{-\frac{w}{2}}^{\frac{w}{2}} \rho_c |J(x)|^2 dV$$

$$= \frac{\rho_c 2 H_m^2 2}{2\delta_c^2}\int_0^h\int_0^{\frac{w}{2}} \frac{cosh(\frac{2x}{\delta_c}) - cos(\frac{2x}{\delta_c})}{cosh(\frac{w}{\delta_c}) + cos(\frac{w}{\delta_c})} dV = \frac{\rho_c H_m^2 l_c h}{\delta_c}\frac{sinh(\frac{2x}{\delta_c}) - sin(\frac{2x}{\delta_c})}{cosh(\frac{w}{\delta_c}) + cos(\frac{w}{\delta_c})}. \qquad (127)$$

Fig. 62 shows $\delta_c P_E \rho_c H_m^2 h l_c$ as a function of w/δ_c. As w/δ_c increases from 0, P_E increases from 0, reaches the maximum values, decreases to minimum value, increase

again to a maximum, and so on.

Taking the derivative of P_E with respect to w/δ_c and setting it to zero

$$\frac{dP_E}{d(\frac{w}{\delta_c})} = \frac{2\rho_c H_m^2 h l_c}{\delta_c} \frac{sinh(\frac{w}{\delta_c}) - sin(\frac{w}{\delta_c})}{[cosh(\frac{w}{\delta_c}) + cos(\frac{w}{\delta_c})]^2} = 0 \tag{128}$$

We get

$$sinh\left(\frac{w}{\delta_c}\right) = 0. \tag{129}$$

Hence, the maximum and minimum values of P_E occur at

$$\left(\frac{w}{\delta_c}\right) = n\pi. \tag{130}$$

where n is the integer.

The largest maximum value of P_E occurs for n =1, resulting in the most lossy lamination thickness

$$wp_{E(max)} = \pi\delta_c = \sqrt{\frac{\pi\rho_c}{\mu_c f}}. \tag{131}$$

Substitution of (131) into (127) gives the maximum time-average eddy-current total power loss

$$P_{E(max)} = \frac{\rho_c H_m^2 h l_c}{\delta_c} \frac{sinh(\pi)}{cosh(\pi) - 1} = \frac{1.09 H_m^2 h l_c}{\delta_c} = \frac{1.09 B_m^2 h l_c}{\mu_c^2 \delta_c} = \frac{1.09 B_m^2 h l_c}{\mu_c} \sqrt{\frac{\pi\rho_c}{\mu_c f}}. \tag{132}$$

Using (124)

$$\frac{d^2 P_E}{d(\frac{w}{\delta_c})^2} = \frac{2\rho_c H_m^2 h l_c}{\delta_c [cosh(\frac{w}{\delta_c}) + cos(\frac{w}{\delta_c})]^3}$$

$$\left\{ sinh(\frac{w}{\delta_c}) sin^2(\frac{w}{\delta_c}) - sinh^2(\frac{w}{\delta_c}) sin(\frac{w}{\delta_c}) + \left[1 + cosh(\frac{w}{\delta_c}) cos(\frac{w}{\delta_c})\right] \left[sinh(\frac{w}{\delta_c}) + sin(\frac{w}{\delta_c})\right] \right\}. \tag{133}$$

Hence,

$$\left.\frac{d^2 P_E}{d(\frac{w}{\delta_c})^2}\right|_{(\frac{w}{\delta_c}) = n\pi} = (-1)^n \frac{2\rho_c H + m^2 h l_c}{\delta_c} \frac{sinh(n\pi)}{[cosh(n\pi) + (-1)^n]^2}. \tag{134}$$

For odd values of $n(n = 1, 3, 5, ...)$,

$$\frac{d^2 P_E}{d(\frac{w}{\delta_c})^2} < 0 \tag{135}$$

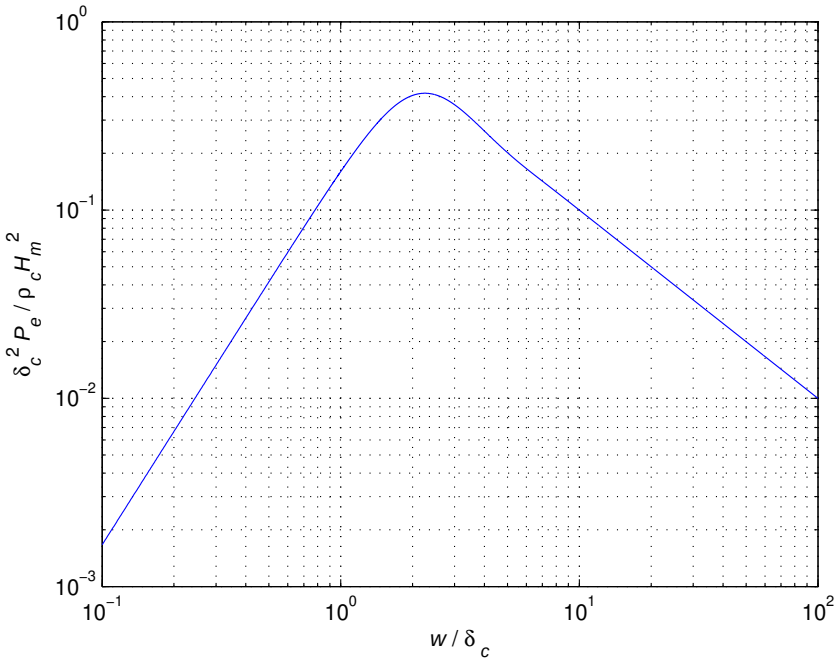

Figure 63: Plot of $\delta_c P_e \rho_c H_m^2 h l_c$ as a function of w/δ_c.

resulting in maximum values of P_E. For even values of $n (n = 2, 4, 6, ...)$,

$$\frac{d^2 P_E}{d(\frac{w}{\delta_c})^2} > 0 \tag{136}$$

yielding the minimum values of P_E. For $n = 2$,

$$w_{P_{E(min)}} = 2\pi\delta_c = 2\sqrt{\frac{\pi\rho_c}{\mu_c f}} \tag{137}$$

and

$$P_{E(min)} = \frac{\rho_c H_c^2 h l_c}{\delta_c} \frac{sinh(2\pi)}{cosh(2\pi)+1} = 0.996 \frac{\rho_c H_c^2 h l_c}{\delta_c}. \tag{138}$$

The time-average eddy-current power loss per unit volume at any frequency is

$$P_e = \frac{P_E}{V_c} = \frac{\rho_c}{2V_c} \int_{-\frac{w}{2}}^{\frac{w}{2}} |J|^2 dx = \frac{\rho_c}{l_c h w} \int_0^{\frac{w}{2}} |J|^2 dx$$

$$= \frac{\rho_c H_m^2}{w\delta_c} \frac{sinh(\frac{w}{\delta_c}) - sin(\frac{w}{\delta_c})}{cosh(\frac{w}{\delta_c}) + cos(\frac{w}{\delta_c})} = \frac{\rho_c H_m^2}{\delta_c^2(\frac{w}{\delta_c})} \frac{sinh(\frac{w}{\delta_c}) - sin(\frac{w}{\delta_c})}{cosh(\frac{w}{\delta_c}) + cos(\frac{w}{\delta_c})} \quad \left(\frac{\mathrm{W}}{\mathrm{m}^3}\right). \tag{139}$$

Fig. 63 shows $\delta_c P_e \rho_c H_m^2 h l_c$ as a function of w/δ_c.

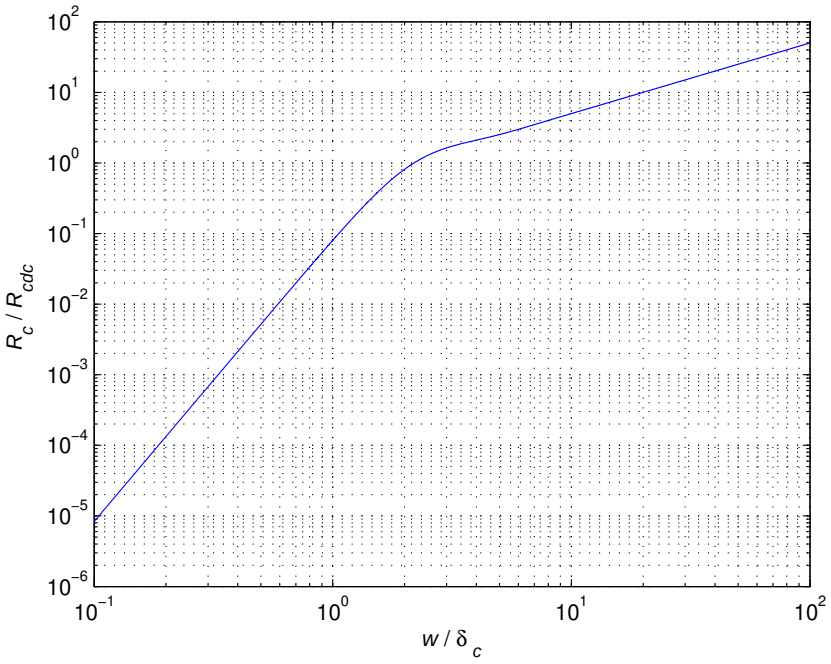

Figure 64: Plot of R_c/R_{cdc} as a function of w/δ_c.

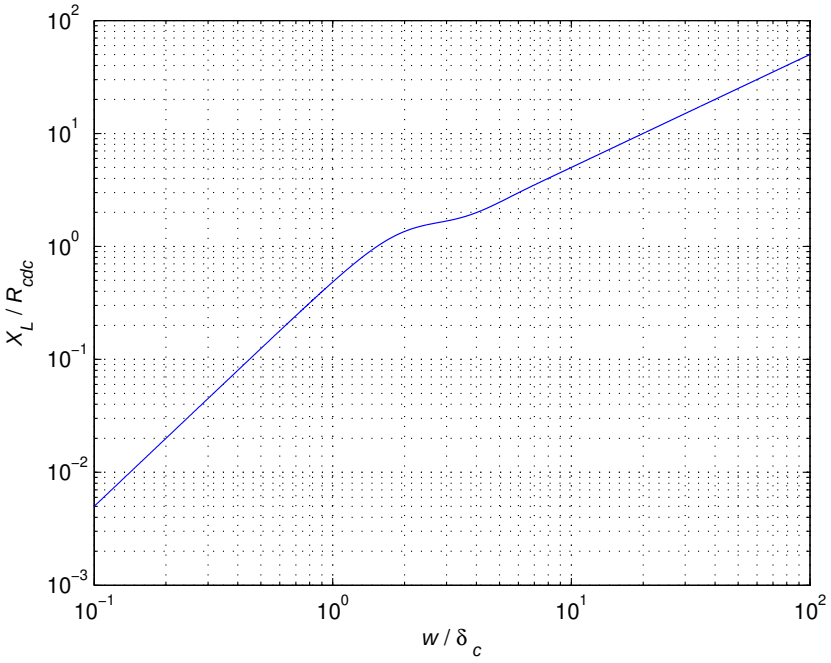

Figure 65: Plot of X_L/R_{cdc} as a function of w/δ_c.

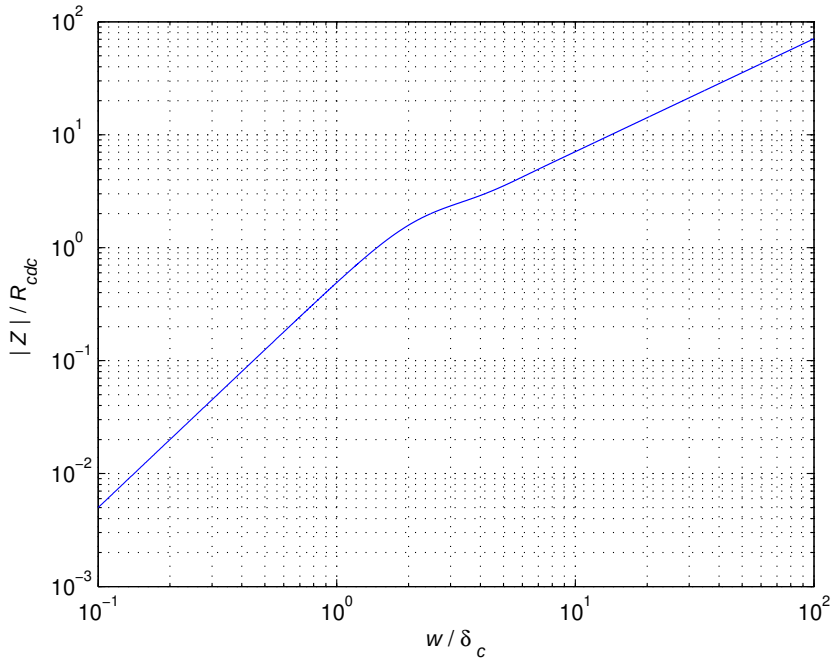

Figure 66: Plot of $|Z|/R_{cdc}$ as a function of w/δ_c.

For low frequencies or a very thin plate($w << \delta_c$)

$$\frac{sinh(\frac{w}{\delta_c}) - sin(\frac{w}{\delta_c})}{cosh(\frac{w}{\delta_c}) + cos(\frac{w}{\delta_c})} \approx \frac{\frac{w}{\delta_c} + \frac{1}{6}(\frac{w}{\delta_c})^3 - \frac{w}{\delta_c} + \frac{1}{6}(\frac{w}{\delta_c})^3}{1+1} \approx \frac{1}{6}\left(\frac{w}{\delta_c}\right)^3. \tag{140}$$

Hence, the time-average eddy-current power loss per unit volume of the core at low frequencies is

$$P_e \approx \frac{\rho_c H_m^2}{w\delta_c}\frac{(\frac{w}{\delta_c})^3}{6} = \frac{\rho_c H_m^2 w^2}{6\delta_c^4} = \frac{\pi^2 B_m^2 w^2 f^2}{6\rho_c} \tag{141}$$

and P_E is approximated by by (127). the eddy-current loss is low when the plates is very thin compared to δ_c. in this case, the magnetic field produced by eddy current is very low. The eddy currents are restricted by lack of space or high core resistivity and are resistance limited.

At high frequencies or very thick plate ($w >> \delta_c$), $e^{w/\delta_c} \approx 0, sinh(w/\delta_c) = cosh(w/\delta_c) \approx e^{w/\delta_c}/2$, resulting in

$$\frac{sinh(\frac{w}{\delta_c}) - sin(\frac{w}{\delta_c})}{cosh(\frac{w}{\delta_c}) + cos(\frac{w}{\delta_c})} \approx \frac{\frac{e^{w/\delta_c}}{2}}{\frac{e^{w/\delta_c}}{2}} = 1. \tag{142}$$

Therefore, the time-average eddy current power loss per unit volume of the core at high frequencies is given by

$$P_e \approx \frac{\rho_c H_m^2}{w\delta_c} = \frac{\rho_c B_m^2}{w\mu_c^2\delta_c} = \frac{H_m^2}{w}\sqrt{\pi\rho_c\mu_c f} = \frac{B_m^2}{w\mu_c}\sqrt{\frac{\pi\rho_c f}{\mu_c}} \quad \left(\frac{\mathrm{W}}{\mathrm{m}^3}\right) \tag{143}$$

and the total time average eddy-current power loss at high frequencies is

$$P_E \approx \frac{\rho_c H_m^2 h l_c}{\delta_c} = H_m^2 h l_c\sqrt{\pi\rho_c\mu_c f} = \frac{B_m^2 h l_c}{\mu_c}\sqrt{\frac{\pi\rho_c\mu_c f}{\mu_c}}. \tag{144}$$

At the high frequencies, the eddy currents are limited by their own magnetic field and are said to be inductance-limited. At low frequencies, P_e is proportional to w^2. in contrast, at high frequencies, $P_e$is inversely proportional to w. thus, there is the worst case of w at which P_e reaches a maximum value [32]. the lamination thickness for the maximum power loss per unit volume occurs at frequencies is

$$w_{p_{e(max)}} \approx 2.252\delta_c \tag{145}$$

resulting in maximum time-average eddy-current power loss per unit volume frequencies is

$$p_{e(max)} \approx 0.4172\frac{\rho_c H_m^2}{\delta_c^2} = 0.4172\frac{\rho_c B_m^2}{\mu_c^2\delta_c^2}. \tag{146}$$

The dc resistance of single lamination is

$$R_{cdc} = \frac{\rho_c h}{w l_c}. \tag{147}$$

the impedance of a lamination is given by

$$\begin{aligned} Z &= \frac{h\rho_c\gamma}{2l_c}coth\left(\gamma\frac{w}{2}\right) = \frac{h\rho(1+j)}{2l_c\delta_c}coth\left(\gamma\frac{w}{2}\right) \\ &= \frac{1}{2}R_{cdc}\left(\frac{w}{\delta_c}\right)(1+j)coth\left(\gamma\frac{w}{2}\right) = R_c + jX_L. \end{aligned} \tag{148}$$

The normalized resistance of lamination is

$$F_R = \frac{R_c}{R_{cdc}} = \frac{1}{2}\left(\frac{w}{\delta_c}\right)\frac{sinh(\frac{w}{\delta_c}) - sin(\frac{w}{\delta_c})}{cosh(\frac{w}{\delta_c}) + cos(\frac{w}{\delta_c})}. \tag{149}$$

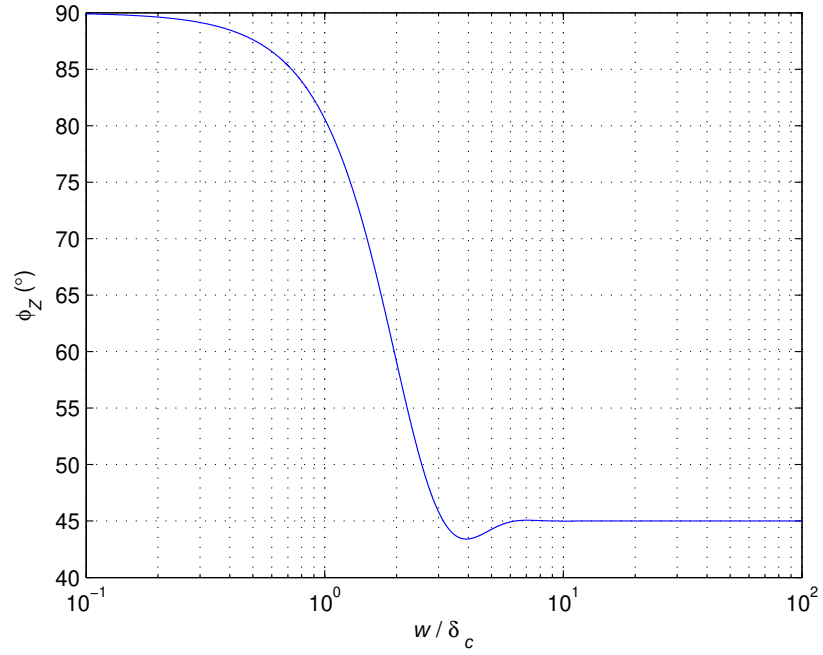

Figure 67: Plot of ϕ_z as a function of w/δ_c.

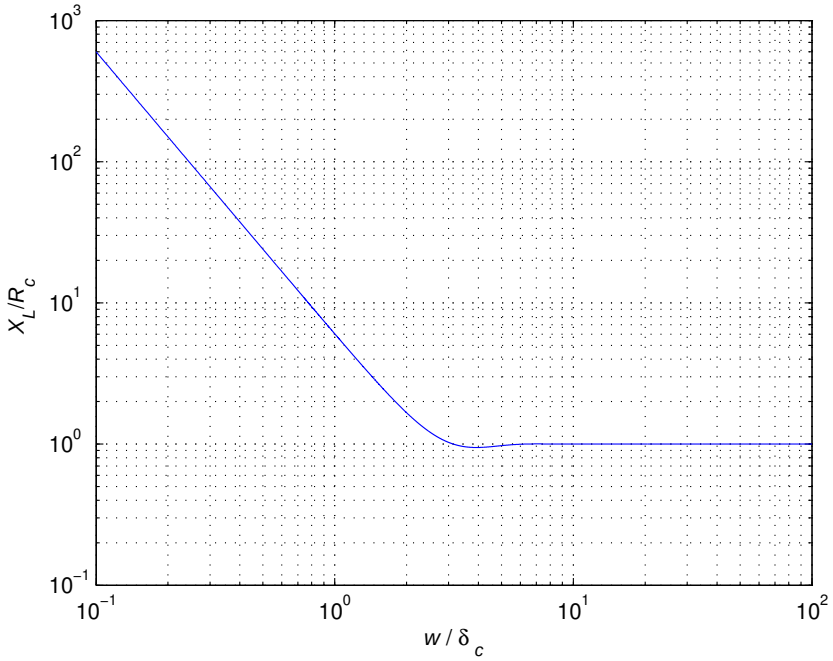

Figure 68: Plot of X_L/R_c as a function of w/δ_c.

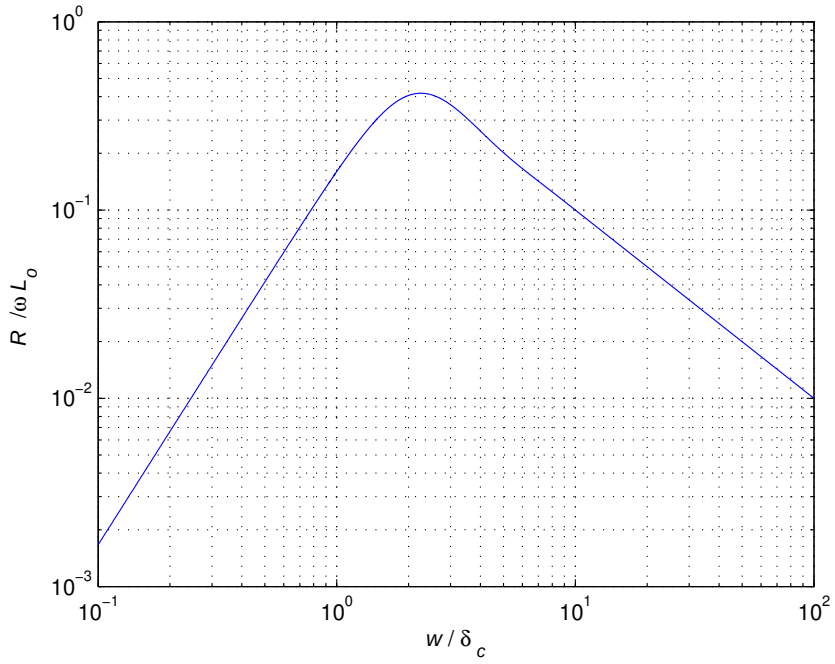

Figure 69: Plot of $R/\omega L_o$ as a function of w/δ_c.

Fig. 64, and 65 show a plot of R_c/R_{cdc} and X_L/R_{cdc} as a function of w/δ_c. The lamination reactance X_L normalized with respect to the core dc resistance R_{cdc} is given by

$$F_X = \frac{X_L}{R_{cdc}} = \frac{1}{2}\left(\frac{w}{\delta_c}\right)\frac{sinh(\frac{w}{\delta_c}) + sin(\frac{w}{\delta_c})}{cosh(\frac{w}{\delta_c}) + cos(\frac{w}{\delta_c})} \tag{150}$$

yielding the core inductance

$$L = \frac{\mu_c h \delta_c}{4 l_c}\frac{sinh(\frac{w}{\delta_c}) + sin(\frac{w}{\delta_c})}{cosh(\frac{w}{\delta_c}) + cos(\frac{w}{\delta_c})} \tag{151}$$

the core impedance is

$$\begin{aligned} Z &= \frac{1}{2}R_{cdc}\left(\frac{w}{\delta_c}\right)\left[\frac{sinh(\frac{w}{\delta_c}) - sin(\frac{w}{\delta_c})}{cosh(\frac{w}{\delta_c}) + cos(\frac{w}{\delta_c})} + j\frac{sinh(\frac{w}{\delta_c}) + sin(\frac{w}{\delta_c})}{cosh(\frac{w}{\delta_c}) + cos(\frac{w}{\delta_c})}\right] \\ &= R_w + jX_L = |Z|e^{j\phi z}. \end{aligned} \tag{152}$$

Fig. 66 and 67 show plots of $|Z|/R_{cdc}$ and ϕ_z. Fig. 68 shows the ratio X_L/R_c as a function of w/δ_c. The magnetic flux flowing through the cross section of a single

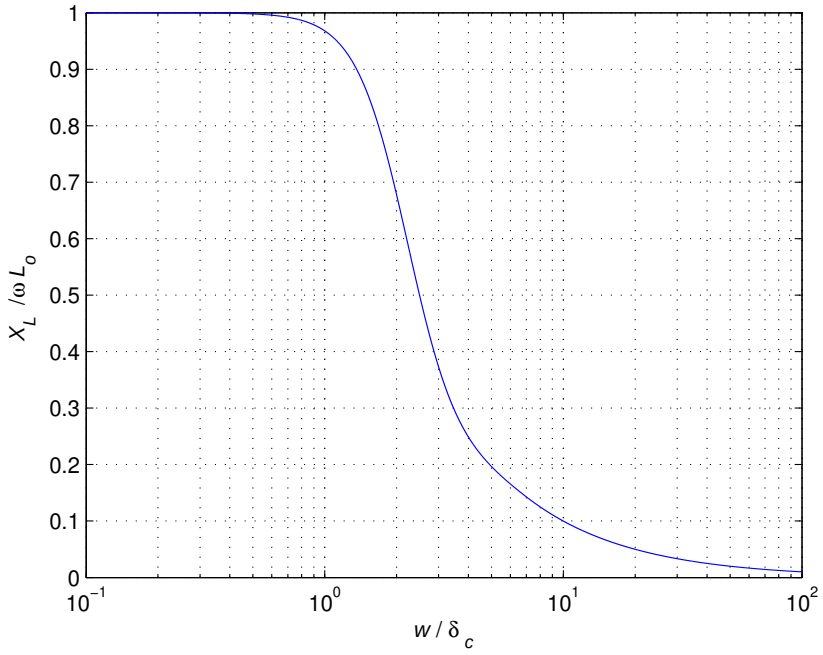

Figure 70: Plot of $X_L/\omega L_o$ as a function of w/δ_c.

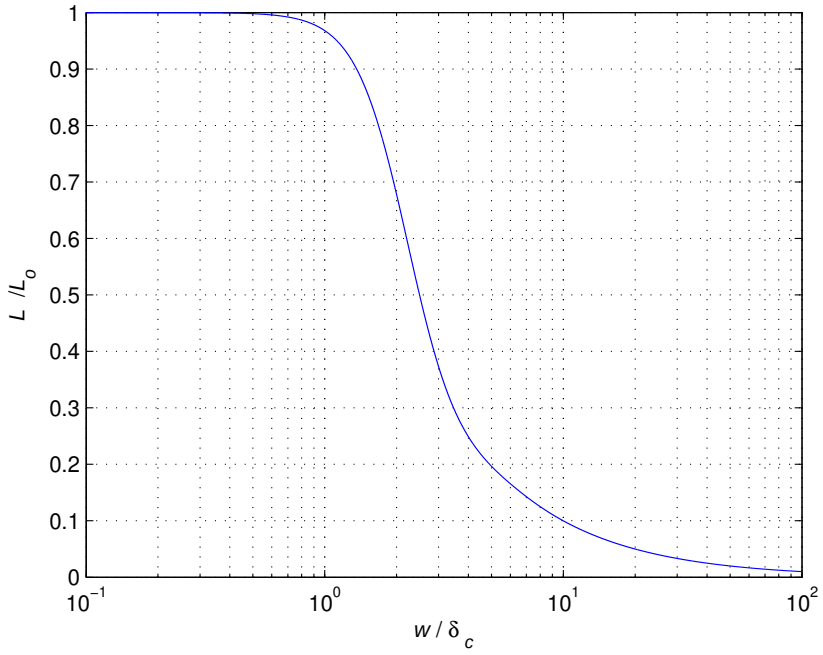

Figure 71: Plot of L/L_o as a function of w/δ_c.

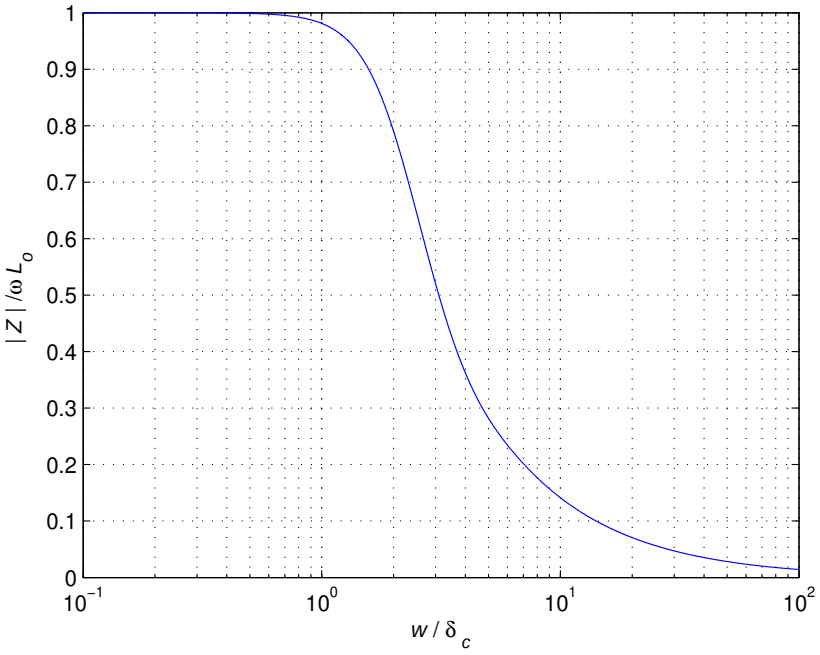

Figure 72: Plot of $|Z|/\omega L_o$ as a function of w/δ_c.

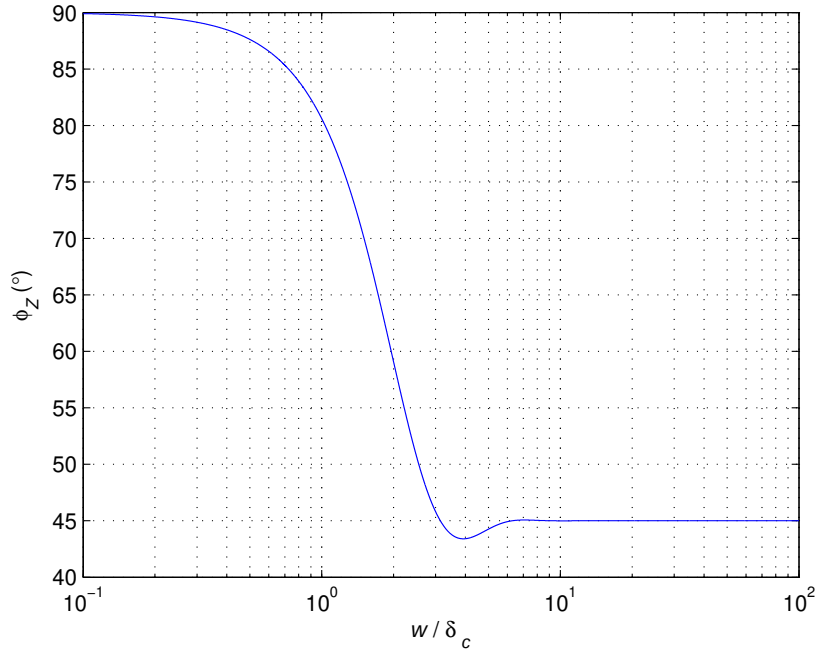

Figure 73: Plot of ϕ_z as a function of w/δ_c.

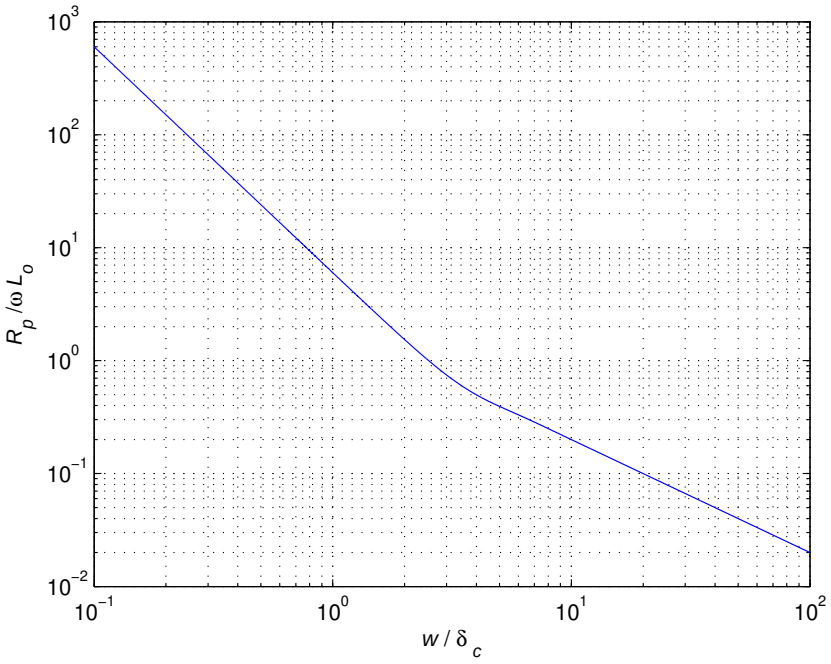

Figure 74: Plot of $R_p/\omega L_o$ as a function of w/δ_c.

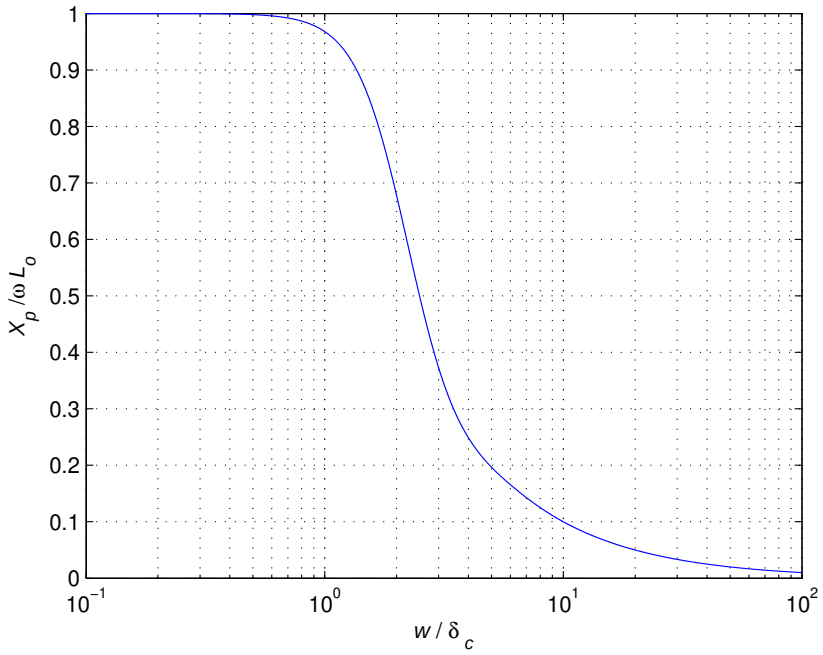

Figure 75: Plot of $X_p/\omega L_o$ as a function of w/δ_c.

laminations given by

$$\phi_{c1} = \int\int_s \mathbf{B}(x)\cdot d\mathbf{s} = \int_0^h dy \int_{-\frac{w}{2}}^{\frac{w}{2}} \mu_c H(x) dx = \frac{h\mu_c H - m}{cosh(\gamma\frac{w}{2})} \int_{-\frac{w}{2}}^{\frac{w}{2}} cosh(\gamma x) dx$$

$$= \frac{2h\mu_c H_m}{\gamma} tanh\Big(\gamma\frac{w}{2}\Big) = \frac{2h\mu_c N I_m}{\gamma l_c} tanh\Big(\gamma\frac{w}{2}\Big) \tag{153}$$

where

$$H_m = \frac{NI_m}{l_c} \tag{154}$$

and N is the number of turns. Since the laminations are close to each other, it can be assumed that the total magnetic flux through n lamination only

$$\phi_c = n\phi_{cl}. \tag{155}$$

The magnetic flux linkage is given by

$$\lambda_c = N\phi = nN\phi_{cl} = \frac{2nN^2h\mu_c}{\gamma l_c} tanh\Big(\gamma\frac{w}{2}\Big). \tag{156}$$

The voltage across the coil is

$$v = \frac{d\lambda_c}{dt} \tag{157}$$

which in the phasor form becomes

$$V = j\omega\lambda_c. \tag{158}$$

hence, the coil impedance is given by

$$Z = \frac{\mathbf{V}}{\mathbf{I}} = \frac{\mathbf{V}}{I_m} = \frac{j\omega\lambda_c}{I_m} = j\omega\frac{2nN^2h\mu_c}{\gamma l_c} tanh\Big(\gamma\frac{w}{2}\Big)$$

$$j\frac{2\omega L_o}{w\gamma} tanh\Big(\gamma\frac{w}{2}\Big) = \omega L_o\Big(\frac{\delta_c}{w}\Big)(1+j)\frac{sinh(\frac{w}{\delta_c}) + jsin(\frac{w}{\delta_c})}{cosh(\frac{w}{\delta_c}) + cos(\frac{w}{\delta_c})} = R + jX_L \tag{159}$$

where the low frequency inductance is

$$L_o = \frac{\mu_c N^2 nwh}{l_c} \tag{160}$$

and

$$tanh(1+j)x = \frac{sinh(2x)jsin(2x)}{cosh(2x)+cos(2x)} = R + jX_L. \tag{161}$$

The series resistance is

$$R = \frac{\omega Lo}{\frac{w}{\delta_c}} \frac{sinh(\frac{w}{\delta_c}) - sin(\frac{w}{\delta_c})}{cosh(\frac{w}{\delta_c}) + cos(\frac{w}{\delta_c})} \tag{162}$$

and the series reactance is

$$X_L = \frac{\omega Lo}{\frac{w}{\delta_c}} \frac{sinh(\frac{w}{\delta_c}) + sin(\frac{w}{\delta_c})}{cosh(\frac{w}{\delta_c}) + cos(\frac{w}{\delta_c})} \tag{163}$$

and the inductance at any frequency is

$$L = \frac{X_L}{\omega} = \frac{Lo}{\frac{w}{\delta_c}} \frac{sinh(\frac{w}{\delta_c}) + sin(\frac{w}{\delta_c})}{cosh(\frac{w}{\delta_c}) + cos(\frac{w}{\delta_c})}. \tag{164}$$

Figs. 69 through 73 show plots $R/\omega L_o, X_L/\omega L_o, L/L_o, |Z|/\omega L_o$ and ϕ_z as functions of w/δ_c. The series equivalent circuit of the coil can be converted into parallel equivalent circuit

$$q = \frac{X_L}{R} \tag{165}$$

$$R_p = R(1+q^2) \tag{166}$$

and

$$X_p = X_L\Big(1 + \frac{1}{q^2}\Big). \tag{167}$$

Figs. 74 and 76 shows plots of $R_p/\omega L_o$ and R_p/ω_o as function of w/δ_c

7 Summary

The power losses in inductors and transformers consist of winding core losses. The core losses consist of hysteresis loss and eddy-current loss. In accordance with Lenz's law, eddy-currents produce their own magnetic field to oppose the original field. There are two kinds if eddy-current: skin effect and proximity effect. Both of these effects cause current crowding. The skin effect is the tendency of (ac) currents to flow near the surface of a conductor, thereby restricting the current to flow to a small part of the total cross-sectional area and increasing the conductor effective resistance. The skin effect takes place when the time-varying magnetic field induces eddy-currents in the conductor itself. The proximity effect is the tendency to change the current distribution in a conductor by magnetic flux produced by current in adjacent conductors. The proximity effect takes place when a second conductor is influenced by a nearby conductor which is carrying a time-varying current.

Eddy-currents are induced whether or not the first conductor carries current. If the second conductor does not carry current, only the proximity effect is present in the second conductor. If the second conductor carries current, then the total eddy current consists of both the proximity eddy current and the skin effect eddy current.

When two conductors carry currents in opposite directions, their magnetic fields are added in the area between them, and subtracted from each other on the outer sides of the wires. This causes an increase of the current density in the conductor areas where the conductors are close to each other, making the currents flow more in these areas. This is called the proximity effect. The anti-proximity effect occurs when two conductors carry currents in the same directions. In this case, the magnetic fields of the conductors are subtracted from each other in the conductor areas where they are close to each other, and added to each others on the outer sides. That makes more current density in the outer areas. For this reason, more currents flow

in these areas. The skin effect eddy-current and the proximity effect eddy-current are orthogonal. The eddy-currents cause a non-uniform distribution of the current density, an increase in the (ac) resistance, an increase the power loss, and a reduction in inductance. According to Lenz's law, the direction of the eddy-currents are such that they oppose the change that causes them. The eddy-current limits the effective capability of a conductor to conduct high-frequency currents. The skin depth has physical meaning. At $x = \delta_w$ the current density in a conductor is reduced to $1/e$ $= 0.37$ of its value on the the surface. As the resistivity ρ decreases and the relative permeability increases, the skin depth δ decreases. In this case, the skin and proximity effect can be neglected, and for $\delta_w < d$ the skin effect increases the (ac) winding resistance over the (dc) winding resistance, increasing the power loss. The proximity effect loss in multiple layer winding is much higher than the skin effect loss. Increasing the distance between conductors in the same layer reduces the proximity-effect power loss. In leaved winding transformers reduced copper loss is caused by the proximity effect at high frequencies, if the current through the primary and secondary windings are in phase. Each lager operates as a single-lager winding and the proximity effect is nearly eliminated. There is an optimum conductor thickness to the conductor or skin depth that leads to the minimum copper loss. To reduce the copper loss due to the proximity effect, it is highly advantageous to reduce the number of winding lagers, increase the winding width, and interleave the winding. Litz wire increases the effective conduction area at high frequencies and thereby reduces the eddy-current loss. Also the eddy-current loss can be reduced by using a laminated iron core with high resistivity. The eddy current loss in a laminated iron core is proportional to f^2, B_m^2, and w^2, and inversely proportional to ρ_c at $w < \delta_w$ for sinusoidal waveform.

7.1 Future Work:

The future work will be investigating the proximity effect when a conductor is surrounded by two or more conductors. Also interpreting the behaviors of the imaginary parts of the eddy currents.

References

1. H. A. Wheeler, "Simple inductance formulas for radio coils ," Proc. IRE, vol. 16, no 10, pp. 1398-1400, October 1928.
2. H. A. Wheeler, "Formulas for the skin effect," Proc. IRE, vol. 30, pp. 412-424, September 1942.
3. C.W.T.McLyman, Transformer and Inductor Design Handbook, 2nd Ed. New York: Marcel Dekker, 1988.
4. A van den Bossche and V .C. Valchev, Inductors and Transformers for Power Electronics, Boca Raton: Taylor and Francis, 2005,
5. F . W Grover, Inductance Calculations, New York, NY: Van Nostrand, 1946, reprinted by New York, NY: Dover Publications, 1962
6. M.J Hole and L.C. Apple, "stray capacitance of a tow-layer air-cord inductor," IEEE Proc, part G, Circuits, Devices and Systems, Vol 125, no. 6, PP. 565-572, December 2005.
7. E.B. Rosa, "calculation of the self-inductance of single-layer coils," Bull. Bureau standards, vol. 2, no2, PP. 161-187, 1906
8. H.M Greenhouse,"Design iof Planar rectangular microelectronic inductors,"IEEE Trans. Parts. Hybrids, packaging, vol. PHP-10, PP. 109, June 1974.
9. P.R. Gray and R. G. Mayer, "Future directions in silicon IC's for RF Personal communications," Proc IEEE 1995 custom Integrated Circuits Conf. May 1995, PP 83-90
10. C P. Yue, C. Ray, J. Lau, T.H. Lee and S.S. Wong, "A Physical model for Planar spiral inductors in silicon," International Electron Devices Meeting Techical Digest, December 1996, PP. 155-185.
11. C.P Yue and S.S Wang, "On-chip spiral inductors with Patterned ground shields for Si-bases RF ICs," IEEE j. sold-state Circuits, Vol. 33,no. 3,

PP. 743-752, May 1998.

12. F Mernyei, F Darrer M. Pardeon, and Sibrai "Reducing the substrate losses of RF integrated inductors," IEEE Microwave and Guided Wave letters, vol. 8. no. 9, PP. 300-3001, September 1998
13. G. Grandi, M. K. Kazimierczuk, Massarini, U. Reggiani,and G. sancineto, "Model of laminated iron-core inductors," IEEE Transactions on Magnetics, vol. 40,, no. 4 PP. 1839-1845, July 2004.
14. K.Howard and M. K. Kazimierczuk, "Eddy-current Power loss in laminated Power cores," Proceeding of the IEEE International Symposium on Circuits and systems, Sydney, Australia, May 7-9,2000, paper III-668, PP. 668-672.
15. A. Reatti and M. K. Kazimierczuk, "comparison of various methods for calculating the ac resistance of inductors," IEEE Transactions on Magnetics, vol 37, PP. 1512-1518, May 2002.
16. C. R. Sullivan "Optimal choice for the number of strands in a litz-wire transformer winding" IEEE transactions on power Electronics Vol. 14, no. 2, PP. 283-291, March 1999.
17. T. L. Simpson, Effect of a conducting shield on the inductance of the an air-core solenoid," IEEE transactions on Magnetics, vol 35, on. 1, PP. 508-515, January1999.
18. H. A. Wheeler, "simple inductance formulas for radio coils"Proc. IRE, vol 16, no. 10, PP 1398-1400, October 1928.
19. H.A. Wheeler,"formulas for the skin effect" Proc IRE, vol 30, PP. 412-424, September 1942.
20. R.G.Medhurst, "HF resistance and self-capacitance of single layer solenoids," Wireless Engineers,pp.35-34, February 1947, and PP. 80-92, March 1947.
21. R. W. Erickson and D. Maksimovic, Fundamentals of power Electronics,

Norwell, MA: Kluwer Academic Publishers, 2001.

22. C. P. Steinmetz, "On the low of hysteresis," AIEE, vol. 9, PP. 3-64, 1992. Also, "A steinmetz contribution to the ac power revolution, "Proc IEEE, vol 72, PP. 196-221, 1984.
23. B. Carsten, "High frequency conductor losses in switch mode magnetics," Proc. of PCI, Munich, Germany, 1986, PP. 161-182.
24. J. P. vandalec and P. D. Ziogos,"A novel approach for the minimizing high frequency transformer copper loss,"IEEE Transactions on Power Electronics. VOL. 3, pp. 266-276, July 1988.
25. A. M. Urling, V. A.Niemela, G. R. skutt, and T. G. Wilson, "characterizing high frequency effects in transformer winding: A guide to several significant papers," IEEE Transactions on Power Electronics Specialists Conference, 1989, PP. 373-385.
26. P. J. Dowell, "Effects of eddy currents in transformer winding," Proc. IEEE, vol . 113, no. 8, pp. 1387-1394, August 1966.
27. A. Kennelly, F. laws, and P. Pierce, "Experimental research in skin effect in conductors," Trans. AIEE, vol. 34, p. 1915, 1915.
28. J. Lammeraner and M. Stafl, Essy Current, Cleveland: CRS Press, 1966.
29. J. Ebert, "Four terminal parameters of HF inductors," Bull. Acad. Polan. Sci. Ser. Sci. Techn. no. 5, 1968.
30. E. C. Snellling, Soft Ferrite: Properties and Applications, London: Iliffe Books Ltd, 1969.
31. R. L. Stall, The Analysis of Eddy Currents, Oxford: Clarendon Press, 1974, pp. 21-27.
32. W. T. McLyman, transformer and Inductor Design Handbook, 3rd Ed. New York: Marcel Dekker, 2000.

33. J. K. Watson, Applications of Magnetism, Ganainesville, 1985.

34. J. C. Maxwell, A Treatise of Electricity and Magnetism, 3rd. Ed. New York, NY: Dover Publishing, 1997

35. J. A. Ferreia, Electromagnetic Modeling of Power Electronic Converters, Boston: Kluwer Acaemic Publisher, 1989.